Contrib Mineral Petrol (2007) 154:455–477
DOI 10.1007/s00410-007-0203-y

ORIGINAL PAPER

Compositional variations and heterogeneity in fertile lithospheric mantle: peridotite xenoliths in basalts from Tariat, Mongolia

Dmitri A. Ionov

Received: 12 December 2006 / Accepted: 3 April 2007 / Published online: 26 April 2007

Abstract Clinopyroxene-rich, poorly metasomatised spinel lherzolites are rare worldwide but predominate among xenoliths in five Quaternary basaltic eruption centres in Tariat, central Mongolia. High-precision analyses of the most fertile Tariat lherzolites are used to evaluate estimates of primitive mantle compositions; they indicate $Mg\#_{PM}$ = 0.890 while lower Mg# in the mantle are likely related to metasomatic enrichments in iron. Within a 10 × 20 km area, and between ~45 and ≥60 km depth, the sampled xenoliths suggest that the Tariat mantle does not show km-scale chemical heterogeneities and mainly consists of residues after low-degree melt extraction at 1–3 GPa. However, accessory (<1%) amphibole and phlogopite are unevenly distributed beneath the eruption centres. Ca abundances in olivine are controlled by temperature whereas Al and Cr abundances also depend on Cr/Al in coexisting spinel. Comparisons of conventional and high-precision analyses obtained for 30 xenoliths show that high-quality data, in particular for whole-rocks and olivines, are essential to constrain the origin of mantle peridotites.

Keywords Peridotite xenolith · Spinel lherzolite · Major elements · Mantle heterogeneities · Primitive mantle

Communicated by J. Hoefs.

Electronic supplementary material The online version of this article (doi:10.1007/s00410-007-0203-y) contains supplementary material, which is available to authorized users.

D. A. Ionov (✉)
LTL, UMR-CNRS 6524, Département de Géologie,
Université J. Monnet, 23 rue P. Michelon,
42023 Saint-Etienne Cedex 2, France
e-mail: dmitri.ionov@univ-st-etienne.fr

D. A. Ionov
Max-Planck-Institut für Chemie, Postfach 3060,
55020 Mainz, Germany

D. A. Ionov
School of Earth Sciences, Macquarie University,
Sydney, Australia

Introduction

Our knowledge of the structure and composition of the lower continental lithosphere remains fragmentary in spite of recent advances in petrologic, experimental and geophysical studies of the deep Earth. Xenoliths in volcanic rocks and mantle fragments exposed at the surface by tectonic processes are direct samples of the upper mantle and remain the only reliable source of information on its mineralogy, chemical composition and microstructures. Those samples, however, only characterize relatively small volumes of the mantle at a specific moment in time. A xenolith suite, in particular, may represent wall rocks within a limited portion of the ''plumbing system'' of a single volcano; it is not uncommon that xenolith suites collected close to each other in the same volcanic field differ significantly in modal and chemical composition (e.g., Ionov et al. 2005c; Xu et al. 2003). Thus, it is not clear, a priori, whether the range of rock types and compositions (or their averages) found in a single xenolith suite could be taken as representative either of a complete lithospheric cross-section at a given site or of a laterally broader mantle domain.

In order to adequately characterize a large mantle domain, considering that it may be heterogeneous in three-dimensional (3D) space, the mantle should be sampled to address possible lateral and vertical heterogeneities. To

ensure representative lateral sampling, one needs to collect xenoliths (in sufficient numbers) from several nearby eruption centres with similar age. To explore depth-related variations, it is necessary to outline the position of each xenolith in a lithospheric cross-section; the latter is only possible if a local pressure-temperature gradient (geotherm) at the time of eruption is established through studies of garnet-bearing xenoliths that enable pressure estimates.

One of few off-craton localities worldwide where these conditions can be met is Tariat in central Mongolia (Fig. 1a). Several late Cenozoic alkali basaltic lava flows and eruption centres in an area of approximately 20 km by 30 km (Fig. 1b) are known to carry xenoliths of deep-seated rocks (Barry et al. 2003; Ionov et al. 1998; Kepezhinskas 1979). Importantly, a local geotherm has been established (Ionov et al. 1998) based on garnet-bearing peridotite and pyroxenite xenoliths from Shavaryn–Tsaram (Fig. 1b), the eruption centre with the most abundant and diverse xenoliths. Only fragmentary data are available so far on mantle xenoliths from elsewhere in the Tariat area (Ionov et al. 1998; Kepezhinskas 1979).

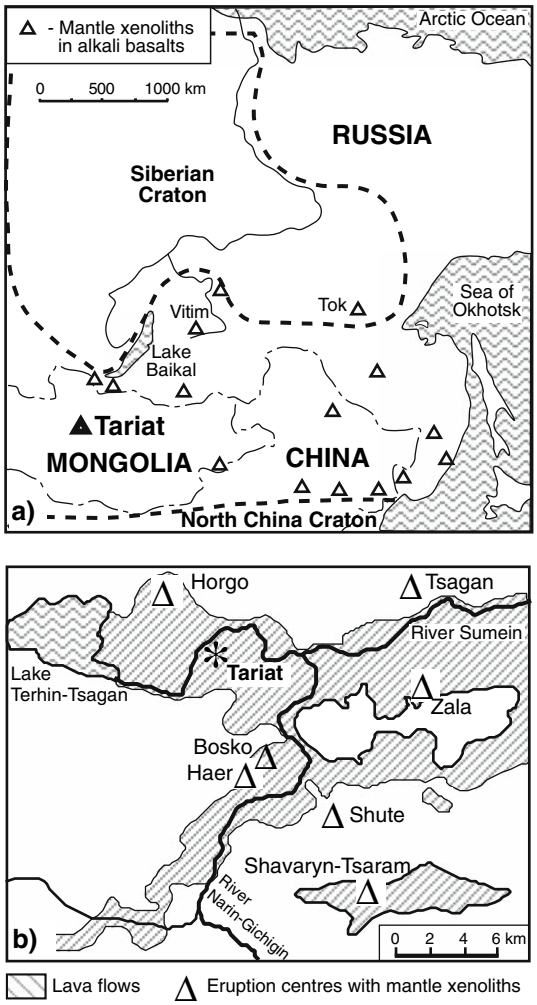

Fig. 1 **a** Sketch map of central and north-east Asia with major occurrences of mantle xenoliths in Cenozoic basalts. **b** Location map for the Tariat region. *Hatched areas* are lava flows (mainly in topographic lows); *triangles* are eruption centres with mantle xenoliths (Ionov et al. 1998; Kepezhinskas 1979)

Here, I report new petrographic and major element data for peridotite xenoliths from four eruption centres in the Tariat area. Minerals and whole-rocks were analysed using both conventional and high-precision techniques to better evaluate analytical uncertainties in peridotite studies and their effects on estimates of mantle composition. A major goal of this work is to characterize the lithospheric mantle in the Tariat area in 3D space and explore its heterogeneity on a km-scale. These data may serve as inputs in any geophysical, tectonic and petrologic modelling of the mantle in central Asia, which has attracted much attention in the last three decades (e.g., Barry and Kent 1998; Delvaux et al. 1995; Petit et al. 2002; Priestley et al. 2006; Windley and Allen 1993; Zorin 1999). In a more general sense, detailed 3D information on mantle domains is essential to address the origin and evolution of the continental lithospheric mantle (CLM) in relation to tectonic settings and geologic history.

An additional benefit of studying Tariat xenoliths is that they come from a very fertile CLM domain. Earlier work on xenoliths from Shavaryn–Tsaram (Ionov 1986; Press et al. 1986) mainly found peridotites that had experienced low degrees of partial melting and metasomatism; some of them have compositions close to primitive mantle estimates (McDonough and Sun 1995; Palme and O'Neill 2003). Such xenolith suites are rare the world over (Ionov et al. 1993; Jagoutz et al. 1979; Xu et al. 2000). The earlier work did not show if such compositions are unique for Shavaryn–Tsaram or whether they characterise a large-scale mantle domain. This study proves that fertile lherzolites are typical for the mantle beneath an area of at least 10×20 km in the Tariat region and provides new constraints on major element composition of primitive mantle.

Geological setting and samples

The Tariat volcanic field (named after a local district centre, Fig. 1b) is situated on the northern slopes of the Hangai Mountains (elevations 1,900–2,700 m) in central Mongolia (Barry et al. 2003; Ionov et al. 1998; Kepezhinskas 1979). That area has recently experienced major uplifting and strike-slip faulting (Cunningham 2001; Tapponier and Molnar 1979) but the basaltic volcanism does not appear to be related to a modern rift system. Rather, it can be viewed

as part of a broad and diffuse belt of Cenozoic volcanism that encompasses southern Siberia, central and SE Mongolia and NE China (Barry et al. 2003; Kepezhinskas 1979; Yarmolyuk et al. 1995). Volcanic activity in the Tariat area started in the Pliocene (6–8 m.y. ago) and continued until a few thousand years ago (the Horgo volcano) (Barry et al. 2003; Genshaft et al. 1990; Kepezhinskas 1979). Basaltic lavas have filled topographic lows to produce broad flat-bottom valleys, with rivers Sumein (Sumyn) and its tributary Gichigin running in narrow canyons (Fig. 1b). Several eruption centres (cinder and lava cones) can be recognised in the vicinity of the lava field.

The Shavaryn (Savariin)–Tsaram volcanic breccia outcrop has long been known as a site with abundant mantle and lower crustal xenoliths (Ionov 1986; Ionov et al. 1998; Press et al. 1986; Stosch et al. 1995; Stosch et al. 1986). Kepezhinskas (1979) and Barry et al. (2003) also reported finds of mantle xenoliths in the pyroclastic deposits of the Horgo volcano and lavas along the rivers Narin-Gichigin and Sumein (Fig. 1b). However, apart from the Shavaryn–Tsaram samples, almost no petrologic data on mantle xenoliths from elsewhere in the Tariat area have been published in international literature.

Xenoliths for this study were collected in four eruption centres (Fig. 1b): Zala, Haer, Shute and Tsagan. The English transcriptions of those geographic names are chosen to render, as closely as possible, those used by the local Mongol population (Ionov et al. 1998). In some cases, they may differ from those on Russian topographic maps used in the field (e.g. Zala instead of Dsala-Tolgoi). The xenoliths at Zala are the largest of these four localities (reaching 15 cm) and most abundant. At each site, all mantle xenoliths >3–4 cm in size, which appeared least altered, were collected; their numbers ranged from about 30 for Tsagan and Shute to some 70 at Zala. One sample was taken in a side vent (Bosko) of the Haer eruption centre.

Sample processing and analytical techniques

The samples were sliced with a rock saw and inspected under binocular microscope. Over 70 peridotite xenoliths were thin-sectioned. Of the >70 samples, 30 were selected for whole-rock studies based on their size (sufficient to obtain >100 g of clean crushed material), low degrees of alteration and the absence of basaltic veins. Their rims were removed and the interiors crushed in a bench-top jaw crusher, carefully cleaned after each sample to avoid cross-contamination. Splits of the crushed whole-rock samples were ground in agate mortars to fine powder. Minerals were hand-picked from 0.5–1.0 mm size fractions of another split to produce polished grain mounts for electron probe micro-beam analyses (EPMA).

Two sets of analytical data were obtained. The first one is based on conventional EPMA and X-ray fluorescence (XRF) methods. Mineral compositions in over 70 xenoliths (listed in Table 1) were determined from polished thin sections by wavelength-dispersive EPMA at Macquarie University (MU) with a Cameca SX50 instrument at an accelerating voltage of 15 kV and sample current of 20 nA. Counting times were 10 s for peaks and 5 s for background on each side of the peak. Standards were natural and synthetic minerals and matrix corrections were by the PAP method. Attention was given to establishing heterogeneities and zoning patterns of pyroxenes (core-rim profiles were run in selected samples) and their relationships to textural position and grain size. A small number of samples were analysed on a Cameca SX-100 at the Service Microsonde Sud, Université Montpellier II. Major elements in bulk rocks were determined in 1996–1997 at MU by XRF using high-dilution (1:10) glass fusion discs as described by O'Reilly and Griffin (1988).

The second set of data was obtained using high-precision methods designed for peridotite analyses. Olivine and spinel were run in grain mounts by EPMA on a Jeol JXA8200 at Max-Planck-Institut für Chemie (Mainz) using 20 kV accelerating voltage, 20 nA current and extended counting times, e.g. 120 s for Ca, Al, Cr, Ni, Mn and Fe. Calibration was done on wollastonite (Ca), San Carlos olivine (USNM 111312/444, Jarosewich et al. 1980) (Si, Mg, Fe), rodonite (Mn) and oxides; ZAF correction was applied. The San Carlos olivine was also measured for control in duplicate after every 20–40 analyses to yield repeatability ($\pm 1\sigma$) of 0.2% for Mg, 0.4% for Fe, 1.2% for Ni, 4% for Mn and Ca, 10–20% for Al and Cr, and 0.03% for Mg# [$Mg/(Mg + Fe)_{at}$] (Ionov et al. 2005c; Sobolev et al. 2005). Similarly, a chromite standard was repeatedly measured as an unknown for control, together with Tariat spinels.

The contents of major and minor elements in whole-rock peridotites were determined by wavelength-dispersive XRF spectrometry at J. Gutenberg University, Mainz. The rock powders were first ignited for ≥3 h at 1,000°C to turn all FeO into Fe_2O_3 and expel water and CO_2. Glass beads produced by fusing 0.8 g of ignited powders with 4.8 g of dried LiB_4O_7 (1:7 dilution) were analysed on a Philips PW1404 instrument using ultramafic and mafic reference rock samples as external standards. Reference samples JP-1 and UBN were analysed as unknowns to control accuracy, with results close to the recommended values. Full duplicate and replicate analyses done in the same sample series typically reproduced within ±0.1% of averages for Si and Mg, ±0.7% for Ti, Al, Cr, Fe, Mn, Ni, Ca and ±5% for Na. The technique has been shown to yield improved accuracy and precision compared to conventional XRF analyses of the same samples judging from reproducibility of

Table 1 A summary of petrographic data, temperature estimates, Mg# in olivine and Cr# in spinel for peridotite xenoliths from four Tariat eruption centres

Sample no	Petrography			Temperature estimates		Minerals		Site, sa. no.	Petrography			Temperature estimates		Minerals	
	Micro-structure	Spongy cpx	Minor phases	Wells core-rim	Ca-in opx core-rim	Mg# in ol	Cr# in sp		Micro-structure	Spongy cpx	Minor phases	Wells core-rim	Ca-in opx core-rim	Mg# in ol	Cr# in sp
Zala								Haer							
Z-5	Pr-porph	Rare		945–960	939–976	0.892	0.089	Hr-2	Pr-moz	Comm	ap?	983–1004	999–1021	0.880	0.080
Z-6				939–981	928–970	0.894	0.077	Hr-4	Pr, linear		fl-inc	856–877	878–895	0.893	0.111
Z-7	Pr	Rare		1053–1085	1050–1086	0.893	0.098	Hr-6	Pr, linear	Rare	ap, fl-inc	965–1002	959–997	0.890	0.126
Z-8	Pr-porph	Rare	Cracks	989–1035	976–1037	0.893	0.110	Hr-9	Pr	Rare		966–968	983–996	0.891	0.082
Z-9	Pr	Comm		1034–1068	1037–1068	0.896*	0.213	Hr-10	Pr	Rare		929–971	918–951	0.891	0.088
Z-10				950–967	938–963	0.896	0.093	Hr-11	Pr	abund	gl patch	916, 970	929	0.888	0.094
Z-11	Pr	Rare		1006–1050	1023–1064	0.887	0.093	Hr-12	Pr	Rare	phl vein	937–961	902–945	0.889	0.078
Z-12	Pr	Rare	fl-inc	1049–1062	1057–1079	0.896	0.124	Hr-16	Pr-moz	Rare	am	907–936	920–960	0.888	0.073
Z-13	Pr	Rare		930–964	952–979	0.896	0.126	Hr-18	Tab-moz	Rare		854–859	880–870	0.896	0.101
Z-14				1026–1047	1040–1070	0.888	0.094	Hr-19	Pr-porph	Rare		917–953	928–944	0.888	0.075
Z-15	Pr-porph	Abund		993–1039	995–1030	0.894	0.086	Hr-20	Pr-porph	abund	phl, fl-inc	970–983	955–973	0.890	0.086
Z-16	Pr	Abund	feldspar	946–939	932–967	0.890	0.094	Hr-21	Pr-porph	Comm		914–953	925–939	0.889	0.083
Z-17	Pr-moz	Abund	fl-inc	914–933	922–969	0.893	0.087	Hr-22	Pr	Comm		949–990	952–984	0.888	0.088
Z-18				1055–1072	1037–1072	0.888	0.086	Hr-25	Pr	Comm	phl, gl		963–1019	0.881	0.081
Z-19	Pr-moz	Rare		919–939	912–958	0.893	0.096	Hr-26	Pr-moz	Rare		973–993	973–1003	0.889	0.080
Z-20				942	927–955	0.891	0.093	Hr-32	Pr-moz	Romm	fl-inc	971–1001	966–993	0.889	0.085
Z-65	Pr	Abund		908–936	924–942	0.888	0.079	Hr-34	Pr	abund	feldspar	891–935	893–945	0.887	0.074
Z-66	Pr-porph	Comm		928–956	933–988	0.892	0.091	Hr-35	Pr-moz	Rare	gl, fl-inc	933–963	931–975	0.889	0.089
Z-67	Pr-porph	Comm	Cracks	899–921	923–945	0.898	0.113	Hr-40	Pr	Rare	gl veins	961–971	955–979	0.888	0.083
Z-68	Pr-porph		kelyphite	1074–1096	1088–1127	0.891	0.104	Hr-45	Pr-porph	Rare	gl veins				
Z-69	Pr-porph	Abund	fl-inc	1069–1077	1076–1088	0.886	0.091	Hr-46	Pr-porph	Rare	phl	909–917	912–949	0.901	0.133
Z-70	Pr	Abund		883	879–901	0.893	0.086	Tsagan							
Z-71	Pr-moz	Abund		1024–1058	1028–1059	0.892	0.091	Ts-2	Pr-moz	Comm		938–936	920–981	0.895	0.080
Z-72				940–960	935–947	0.891	0.087	Ts-3	Pr-porph	Rare	am	879–902	899–912	0.904	0.131
Shute								Ts-5	Pr-moz	Comm	am	906–951	908–946	0.888	0.080
St-0	Pr	Rare	phl, ilm		964	0.891	0.076	Ts-10	Pr-porph	Rare		916–968	936–983	0.889	0.090
St-2	Pr	Comm	phl	957–988	948–991	0.886*	0.084	Ts-11	Pr-porph				921	0.890	0.082
St-3	Pr	Rare	phl	900–927	894–924	0.894	0.086	Ts-13	Pr-porph		am	908–940	900–931	0.889	0.084
St-4	Pr	Comm	phl	971–993	947–994	0.891	0.087	Ts-14	Pr-moz		am, phl		906–907	0.898	0.086
St-7	Pr	Comm	phl	897–926	895–970	0.900	0.125	Ts-21	Pr	Rare	am, phl	891–940	903–944	0.888	0.081
St-11	Pr-moz		phl vein	850–841	893–871	0.889	0.079	Ts-23	Pr-porph	Rare	am	909–929	897–932	0.889	0.098
St-12	Pr		phl	1003–1032	1004–1041	0.894	0.093	Ts-25	Melted	Abund	Glass	979–952	942–960	0.848	0.082
St-13	Pr	Comm		866–883	881–913	0.903	0.112	Ts-28	Pr	Rare	am	893–943	898–952	0.888	0.075

Table 1 continued

Sample no	Petrography			Temperature estimates		Minerals		Site, sa. no.	Petrography			Temperature estimates		Minerals	
	Micro-structure	Spongy cpx	Minor phases	Wells core-rim	Ca-in opx core-rim	Mg# in ol	Cr# in sp		Micro-structure	Spongy cpx	Minor phases	Wells core-rim	Ca-in opx core-rim	Mg# in ol	Cr# in sp
St-16	Pr-moz	Comm	fl-inc	921–949	931–947	0.888	0.084	Ts-29	Pr	Rare	am, phl	896–924	908–949	0.886	0.084
St-19	Pr	Rare		882–932	896–916	0.889	0.082	Ts-31	Pr	Comm	am	867–938	903–923	0.894	0.091
St-21	Pr	Comm	phl	959–1006	936–979	0.894	0.098	Ts-32	Pr-moz	Abund	Glass	917	887	0.899	0.177
St-23	Pr	Rare	phl, ap	955–989	948–964	0.891	0.077	Ts-33	Melted	no cpx	Glass				
Bosko	Pr-porph				1066–1087	0.890	0.093	Ts-34	Pr-moz	Rare	am	889	902–919	0.886	0.080

Sample numbers are underlined for xenoliths analysed for whole-rock compositions. Spongy cpx contents are visual estimates relative to total cpx: rare <5%, common 5–30%, abundant 30–99%. Mineral compositions are from analyses done in thin sections at Macquarie University and Université Montpellier II. Mg#, Mg/(Mg + Fe)$_{at}$; Cr#, Cr/(Cr + Al)$_{at}$. Mg# values with asterix are for zoned olivine. Temperature estimates (°C) are after Wells (1977) and Ca-in-opx method of Brey and Köhler (1990) assuming P = 1.5 Gpa. Blank entries, not detected or not determined

Ol olivine, *cpx* clinopyroxene, *opx* orthopyroxene, *sp* spinel, *am* amphibole, *phl* phlogopite, *ap* apatite, *gl* glass, *ilm* ilmenite, *fl-inc* fluid inclusions. Microstructures: *pr* protogranular, *moz* mosaic, *tab* tabular, *porph* porphyroclastic

duplicates, analyses of reference materials as unknowns and less scatter on element co-variation plots (Ionov et al. 2005a). Fourteen Tariat peridotites were analysed using low dilution (1:5) beads and a similar technique at the Niigata University (Takazawa et al. 2003); 12 duplicates analysed both at Mainz and Niigata match each other very well (Ionov et al. 2005c).

Petrography

A list of samples in this study is given in Table 1 together with some petrographic data as well as temperature (T) estimates, $Mg\#_{Ol}$ [Mg# in olivine] and $Cr\#_{Sp}$ [Cr/(Cr + Al)$_{at}$ in spinel] from conventional EPMA. All the xenoliths are medium- to coarse-grained spinel lherzolites except lherzolite Z-68 from Zala with kelyphite (after garnet) surrounding spinel (Ionov et al. 1998). Modal clinopyroxene (cpx) ranges from 8 to 20%; cpx-rich rocks are typical (Fig. 2d, e). Microstructures range from protogranular (Fig. 2a, b) to granoblastic; protogranular and mosaic domains coexist in some xenoliths (Fig. 2c). Spinel ranges from coarse (5–10 mm) poikilitic (Fig. 2a) to small interstitial grains; vermicular spinel is common at olivine and opx grain boundaries (Fig. 2b, e). Strained grains, exsolution lamellae in pyroxenes and foliation are rare. Two xenoliths contain abundant, sub-parallel micro-fractures (Fig. 2d).

Cpx grains in some samples (listed in Table 1) are rimmed with fine-grained, spongy aggregates of secondary cpx (optically continuous with the parent grain but with lower Na and Al; eTable 1) containing empty vermicular micro-channels (Fig. 2d, e) and rare feldspar (Table 1). Similar spongy cpx were earlier found in other xenolith suites from central and eastern Asia (Ionov 2002; Qi et al. 1995; Wiechert et al. 1997). The amount of the spongy cpx may vary within each sample; in some cases (Fig. 2e) nearly all normal cpx is replaced with the spongy aggregates. Other minerals do not appear to be affected by this process (Fig. 2e) except that adjacent spinel in a few samples (Z-16, Hr-34) is partly corroded. Several Haer xenoliths contain interstitial veins or pockets of silicate glass (Table 1). Three Tsagan xenoliths have large, abundant (up to 25% of the rock) patches of vesicular silicate glass with micro-phenocrysts of olivine, cpx and spinel, and corroded spinel. Similar ''melt pockets'' were earlier described in Shavaryn–Tsaram xenoliths (Ionov et al. 1994).

While microstructures and modal compositions appear to be similar in xenoliths from the four Tariat eruption centres, the xenolith suites at each site can be distinguished by the presence and relative abundances of accessory (<1%) amphibole (amph) and phlogopite (phl) (Figs. 2c, 3)

as well as late-stage interstitial materials. No volatile-bearing minerals have been found in 25 xenoliths from Zala studied in thin sections. Among the 22 Haer xenoliths, only four contain phl and one has amph; silicate glass was found in five samples. Phlogopite is common in the Shute xenoliths (nine out of 12), but no amph has been found. By contrast, ten out of 16 Tsagan xenoliths contain amph while in three of them amph coexists with rare phl; another three Tsagan xenoliths have abundant silicate glass, which may have replaced pre-existing amph (e.g., Yaxley and Kamenetsky 1999). Overall, amph (or its breakdown products) is a typical accessory phase in the Tsagan xenoliths while phl is typical for the Shute suite (Fig. 3). By contrast, Zala xenoliths have no amph or phl but more commonly than for the other suites contain spongy cpx and fluid inclusions in silicate minerals. Apatite was found in two samples from Haer and one from Shute (Ionov et al. 2006). Peridotite xenoliths from the nearby Shavaryn–Tsaram most commonly contain no volatile-bearing minerals, but some were earlier reported to have phl (Ionov et al. 1983; Ionov and Hofmann 1995; Ionov et al. 1998); amph and apatite are very rare (Ionov et al. 1984; Ionov et al. 2006; Ionov et al. 1994; Ionov et al. 1997; Press et al. 1986).

Comparisons of conventional and high-precision analyses

Because EPMA and XRF analyses for many samples in this study are duplicated in two laboratories, the data offer a unique opportunity to double-check the quality of these analyses as well as evaluate some relevant literature data.

Conventional EPMA for olivine, pyroxenes, spinel and accessory phases from over 70 Tariat xenoliths are given in eTable 1 of electronic supplementary material (ESM); high-precision EPMA of olivine and spinel from 30 of those samples are given in Table 2 and eTable 2, respectively. Based on the conventional EPMA, the $Mg\#_{Ol}$ range from 0.886 to 0.898 and $Cr\#_{Sp}$ from 0.073 to 0.126 using 95% (to avoid obvious outliers) of the population (Table 1). The $Mg\#_{Ol}$ based on high-precision data from Mainz (RSD ≤ 0.0006; Table 2) are ~0.005 higher than those from the conventional EPMA; the differences in $Cr\#_{Sp}$ are smaller. The high-precision EPMA define a tighter positive correlation between $Mg\#_{Ol}$ and $Cr\#_{Sp}$ (Fig. 4b) which match better with published data on xenoliths from Shavaryn–Tsaram (Ionov 1986; Press et al. 1986) and appear to be more accurate. Pyroxenes were only run with conventional EPMA because potential gains in

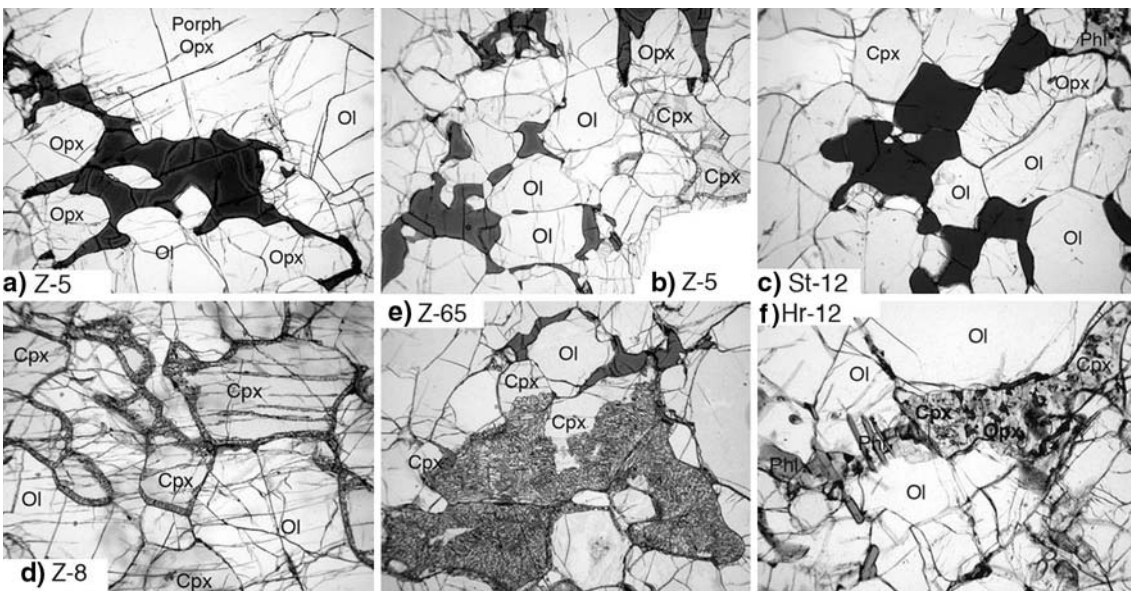

Fig. 2 Photomicrographs of Tariat peridotite xenoliths in plane-polarized transmitted light. Horizontal field of view is 5–6 mm; sample numbers are indicated on each plate. *Ol*, olivine; *Opx*, orthopyroxene; *Cpx*, clinopyroxene; *Phl*, phlogopite. **a** Protogranular microstructure with coarse poikilitic spinel (*dark*) and porphyroclastic Opx (*top* to *centre*). **b** Protogranular medium-grained rock with common curvilinear grain boundaries of Ol and pyroxenes and vermicular interstitial spinel. **c** Transition from protogranular to granoblastic microstructure with triple junctions of olivine grains at 120° and more equant coarse spinel than in **a** and **b**; note interstitial Phl in upper right corner. **d** Sub-parallel micro-fractures in minerals; note spongy Cpx along some cracks in Cpx grains. **e** Nearly complete replacement of coarse Cpx by spongy, (Na,Al)-poor Cpx; note the absence of alteration in interstitial spinel. **f** Metasomatic Phl at grain boundaries and replacing Ol; nearby pyroxene grains are spotted because of spongy domains in the Cpx and spinel exsolution in the Opx (*centre right*)

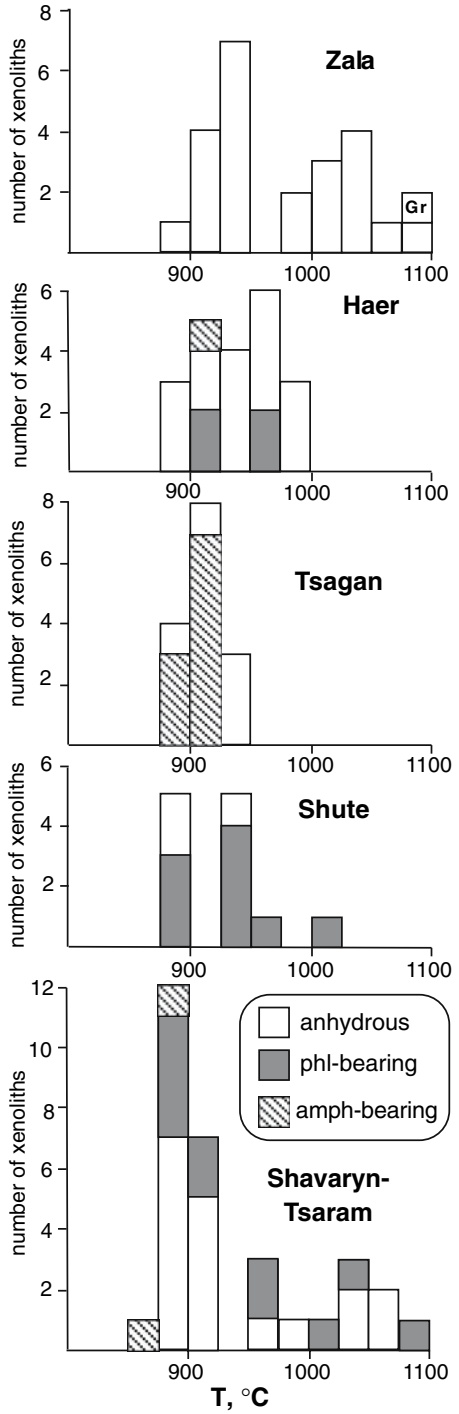

Fig. 3 Histograms of temperature estimates from Ca-opx method (Brey and Köhler 1990) on grain cores for peridotite xenoliths from four Tariat eruption centres in this study (Table 1) and for Shavaryn–Tsaram from literature data (Ionov 1986; Ionov et al. 1983, 1984; Press et al. 1986). *Hatched squares* are for amphibole-bearing xenoliths, *grey squares* are for phlogopite-bearing xenoliths; predominant 'hydrous' mineral (amph) is shown for three Tsagan xenoliths where amph and phl coexist; one Zala xenolith contains garnet (Gr). The share of ''hydrous'' xenoliths at Shavaryn–Tsaram is exaggerated because they have been extensively studied

precision make little sense relative to common core-rim zoning and inter-grain variations.

High-precision bulk rock analyses of 30 Tariat xenoliths are given in Table 3. A complete set of the XRF data relating to this work (including duplicate analyses from MU and Niigata) is provided in eTable 3. Compared to the data from Mainz, the MU values for MgO and Al_2O_3 display more scatter (eFig. 1a); they also tend to be lower and plot off melt extraction trends defined by Horoman peridotites (Takazawa et al. 2000) and experimental results (Herzberg 2004; Niu et al. 1997). On a MgO-FeO diagram (eFig. 1b), the MU analyses of Zala xenoliths show much scatter but do not stray far from the Mainz data field. By contrast, FeO contents in Haer, Tsagan and Shute xenoliths obtained at MU in a different analytical session are systematically higher. Altogether, these differences may be related to recurrent calibration problems and lower precision of the MU data. In addition, volatiles in alteration products present in rock powders run at MU (CMI up to 1.7%; Table 3) may variably 'dilute' the major oxide contents while the Mainz analyses were done on ignited (volatile-free) powders.

The FeO values from MU and Niigata are plotted in Fig. 5 versus the Mainz data for the same samples. The data from Mainz are consistent with those from Niigata, with differences $\leq 0.1\%$ FeO for all 12 duplicated samples and $\leq 0.05\%$ for nine of them. By contrast, the MU FeO values show much more scatter and/or systematic bias relative to 1:1 reference line, with differences >0.3% in eight out of the same 12 samples compared to the Mainz data (Fig. 5). Overall, the XRF data from Mainz and Niigata are more precise and accurate that the earlier conventional results. The dataset from Mainz (supplemented by analyses from Niigata for four samples) is used in the discussion below.

Mineral major element compositions

The xenoliths from Zala, Haer, Shute and Tsagan have very similar ranges of mineral composition (Tables 1, 2, eTable 1). $Mg\#_{Ol}$ in the majority of the Tariat peridotites analysed at Mainz range from 0.891 to 0.902 while $Cr\#_{Sp}$ range from 0.077 to 0.121. These $Mg\#_{Ol}$ and $Cr\#_{Sp}$ values are lower than in abyssal peridotites and in the majority of spinel peridotite xenoliths from other localities in central and eastern Asia and worldwide (Fig. 4a, b).

The high-precision EPMA, together with published data on xenoliths from Shavaryn–Tsaram (Ionov 1986; Press et al. 1986) define a positive correlation between $Mg\#_{Ol}$ and $Cr\#_{Sp}$ (Fig. 4b) suggestive of variable degrees of melt extraction. Five samples (labelled in Fig. 4a, b) plot off the

Table 2 High-precision EPMA (wt.%) of olivine from MPI fuer Chemie, Mainz

Sa. no.	SiO_2	Al_2O_3	Cr_2O_3	FeO	MnO	NiO	MgO	CaO	Total	Mg#	Mg#RSD (%)
Z-5	40.79	0.019	0.007	10.13	0.143	0.368	49.07	0.049	100.6	0.896	0.04
Z-6	40.82	0.014	0.007	10.08	0.140	0.373	49.21	0.050	100.7	0.897	0.04
Z-7	40.81	0.045	0.018	10.00	0.142	0.358	49.14	0.094	100.6	0.898	0.05
Z-8	40.88	0.034	0.014	10.01	0.140	0.372	49.07	0.069	100.6	0.897	0.05
Z-9[a]	40.76	0.039	0.029	10.31	0.134	0.380	48.84	0.084	100.6	0.894	1.02
Z-11	40.77	0.034	0.013	10.26	0.144	0.365	48.85	0.079	100.5	0.895	0.05
Z-12	40.98	0.038	0.017	9.59	0.133	0.365	49.49	0.086	100.7	0.902	0.05
Z-14	40.72	0.033	0.014	10.6	0.145	0.368	48.67	0.081	100.6	0.891	0.05
Z-15	40.81	0.029	0.012	10.14	0.143	0.367	48.95	0.068	100.5	0.896	0.06
Z-16	40.65	0.018	0.011	10.16	0.141	0.375	49.06	0.051	100.5	0.896	0.04
Z-17	40.74	0.014	0.008	10.03	0.139	0.372	49.15	0.048	100.5	0.897	0.05
Z-18	40.74	0.037	0.016	10.40	0.146	0.357	48.90	0.085	100.7	0.893	0.05
Z-65	40.71	0.016	0.006	10.43	0.145	0.368	48.86	0.045	100.6	0.893	0.06
Z-71	40.78	0.034	0.012	10.08	0.138	0.361	49.24	0.078	100.7	0.897	0.03
Z-72	40.72	0.016	0.005	10.26	0.144	0.365	49.01	0.052	100.6	0.895	0.06
Hr-2	40.95	0.026	0.006	11.19	0.152	0.361	48.15	0.066	100.9	0.885	0.03
Hr-4	41.16	0.012	0.002	9.88	0.137	0.372	49.29	0.030	100.9	0.899	0.03
Hr-6	40.98	0.029	0.011	10.47	0.142	0.365	48.66	0.056	100.7	0.893	0.05
Hr-12	41.07	0.011	0.006	10.66	0.147	0.363	48.60	0.045	100.9	0.891	0.04
Hr-18	41.15	0.009	0.006	9.79	0.140	0.371	49.34	0.027	100.8	0.900	0.05
Hr-20	40.90	0.019	0.006	10.37	0.145	0.360	48.80	0.056	100.7	0.894	0.05
Hr-22	40.78	0.023	0.006	10.33	0.146	0.365	48.59	0.058	100.3	0.894	0.05
Hr-25[a]	40.42	0.050	0.008	13.36	0.175	0.361	46.04	0.064	100.5	0.861	1.08
Hr-26	41.06	0.028	0.008	10.35	0.145	0.364	48.90	0.061	100.9	0.894	0.08
Bosko[a]	40.50	0.047	0.016	11.69	0.150	0.344	47.81	0.096	100.6	0.879	1.05
St-0	40.77	0.025	0.008	10.41	0.146	0.367	48.89	0.062	100.7	0.893	0.04
St-3	40.70	0.009	0.006	10.11	0.141	0.375	49.06	0.038	100.4	0.896	0.04
St-23	40.71	0.021	0.008	10.38	0.144	0.369	48.90	0.057	100.6	0.894	0.04
Ts-14	40.86	0.012	0.003	9.99	0.143	0.365	49.19	0.039	100.6	0.898	0.05
Ts-21	40.84	0.007	0.002	10.50	0.145	0.366	48.85	0.042	100.8	0.892	0.05

All data are averages of 6–7 analyses in grain mounts. *RSD*, relative standard deviation (1σ/average) in percent

[a] Heterogeneous Fe distribution (RSD for Mg# >1% compared to ≤ 0.06% in homogeneous olivine) is typical of Fe-enriched Tariat xenoliths

$Mg\#_{Ol}$–$Cr\#_{Sp}$ trend towards lower $Mg\#_{Ol}$; three of them (Z-9, Hr-25 and Bosko) have broad grain-to-grain variations of $Mg\#_{Ol}$ (RSD > 1%; Table 2). Similarly, olivine and pyroxenes in several xenoliths have rims enriched in Fe relative to cores (Table 1, eTable 1). These heterogeneities may be due to late-stage enrichments in iron (hence lower Mg#), which have failed to re-equilibrate by diffusion. Olivines from four Fe-enriched xenoliths plot off the negative Mg#–MnO trend defined by the remainder of the samples (Fig. 4d).

Pyroxenes in the majority of the samples are zoned with lower contents of Al (as well as lower Cr and Na for the cpx) towards the rims; the cpx have lower Ca in the rims whereas opx have higher Ca in the rims (eTable 1). Significant zoning is usually restricted to the outer 50 μm of the grain. Fe-enriched xenoliths as well as rare rocks with abundant amph or phl have less systematic core-rim relationships, i.e. with either higher or lower Al and Ca toward the rims and common inter-grain variations.

The contents of Al_2O_3 in cpx cores (6.5–7.8%) are higher than in abyssal peridotites and the majority of peridotite xenoliths worldwide (Fig. 4c) but similar to the range reported for fertile Shavaryn–Tsaram lherzolites (Ionov 1986; Press et al. 1986). The Tariat cpx usually have moderately high Na_2O (1.6–2.0%) and TiO_2 (0.45–0.75%) typical of fertile mantle (Fig. 6). Cpx from a small number of samples, mainly Fe-enriched and those containing glass veins, have elevated Na_2O (2.1–3.0%; Fig. 6a), with common Na enrichments in the rims (eTable 1); Na-rich cpx were earlier reported from metasomatised Shavaryn–Tsaram xenoliths

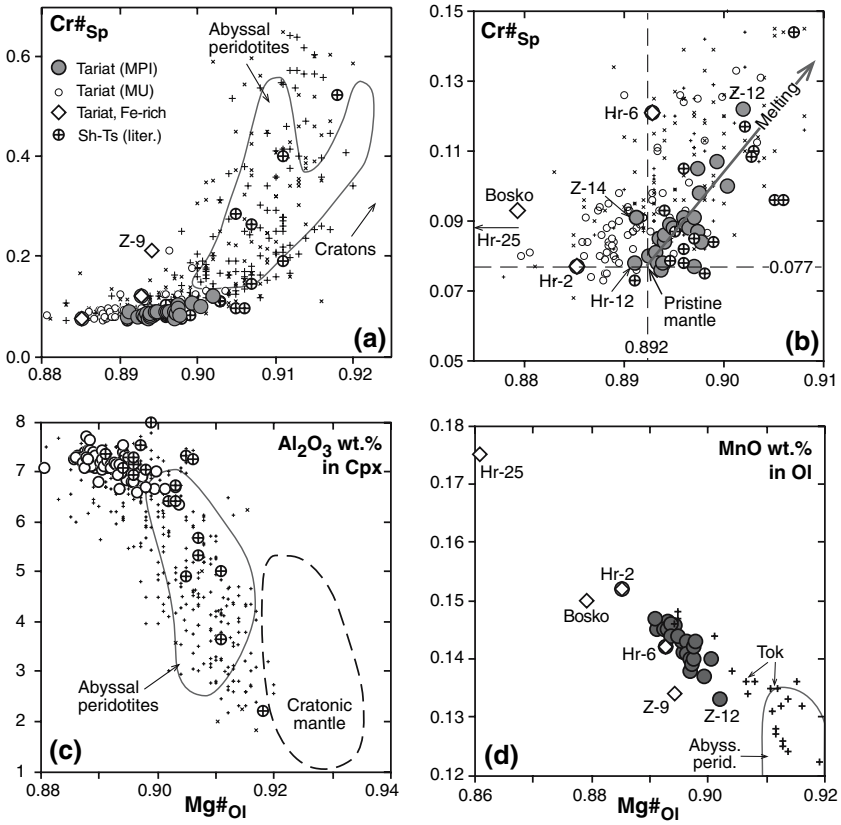

Fig. 4 Plots of $Mg\#_{Ol}$ [$Mg/(Mg + Fe)_{at}$ in olivine] versus $Cr\#_{Sp}$ [$Cr/(Cr + Al)_{at}$ in spinel] (**a**, **b**), Al_2O_3 in cpx (**c**) and MnO in olivine (**d**) for Tariat peridotite xenoliths; large *filled circles*, high-precision EPMA from MPI-Mainz; small *empty circles*, conventional EPMA from Macquarie University (MU) and Université de Montpellier II. Also shown are literature data for spinel peridotite xenoliths from Shavaryn–Tsaram (Sh-Ts, *crossed circles* Ionov 1986; Press et al. 1986), North America (*small diagonal crosses*, Smith 2000), Tok (*crosses* Ionov et al. 2005c) as well as a selection of other xenolith localities in Eurasia (*small crosses*) and fields for abyssal and cratonic peridotites after Ionov et al. (2005c). Fe-enriched Tariat xenoliths are labelled

(Ionov et al. 1994). The Na-rich cpx however are much less common and have lower Cr_2O_3 than those from Tok in SE Siberia (Ionov et al. 2005c). The TiO_2 contents in the cpx are negatively correlated with $Cr\#_{Sp}$; cpx in the Fe-enriched xenoliths are not enriched in Ti compared to the other samples.

Whole-rock major element and modal compositions

High-precision major element compositions of 30 Tariat xenoliths are given in Table 3. The change of mass on ignition (CMI) in whole-rock powders of xenoliths from Haer, Shute and Tsagan ranges from –0.2 to +0.4%, with a good match for samples duplicated at Mainz and Niigata (eTable 3) and thus indicates low degrees of alteration. Mass gain on ignition means that oxidation of FeO to Fe_2O_3 (which can increase the mass up to 0.6% for fresh peridotites with $\sum$FeO ~8%) is more significant than the loss of volatiles (mainly H_2O and CO_2 from alteration products). The most altered samples are found at Zala (CMI from –1.7 to +0.4%). The differences in alteration degrees are not likely to affect major element compositions obtained on ignited (volatile-free) powders.

The xenoliths from the four Tariat eruption centres have similar compositional ranges, e.g. Al_2O_3 from 2.1 to 4.7 wt.% and a more limited range of 3.3–4.4 wt.% Al_2O_3 in 80% of the samples (Fig. 7a). Average whole-rock compositions at each site are also close to each other: 3.6–4.0 wt.% Al_2O_3, 3.0–3.25 wt.% CaO and 38.2% MgO. These values are similar to the ranges earlier reported for representative peridotites from Shavaryn–Tsaram (Press et al. 1986; Spettel et al. 1991) and for garnet and spinel lherzolites from Vitim in southern Siberia (Fig. 7), but are more fertile than for the majority of other basalt-hosted peridotite suites (e.g. McDonough 1990; Pearson et al. 2003) and massif peridotites (Bodinier and Godard 2003).

Modal compositions calculated from whole-rock and mineral analyses by mass balance using least-squares regression are given in Table 3 and plotted in Fig. 8. The great majority of the xenoliths (27 out of 30) are rich in cpx (12–20%) and low in olivine (45–60%). The remainder are moderately refractory rocks with 7–10% cpx and 64–67% olivine. Modal cpx is negatively correlated with modal olivine (Fig. 8b) while the contents of Al, Ca, Si, Ti and Na are negatively correlated with Mg (Fig. 7). These correlations show a good match to modal and chemical trends found earlier in several well-studied but less fertile peridotite series, like the Horoman massif (Takazawa et al. 2000) or xenoliths in basalts from SE Mongolia (Wiechert et al. 1997) and southern Siberia (Ionov et al. 2005c), and

Table 3 High-precision XRF analyses of whole-rock samples and calculated modal compositions (wt. %) for Tariat peridotite xenoliths

	Whole-rock XRF analyses, wt.%:															Calculated mineral abundances, wt.%				
	SiO_2	TiO_2	Al_2O_3	Cr_2O_3	FeO	MnO	NiO	MgO	CaO	Na_2O	K_2O	P_2O_5	Total	Mg#	Ca/Al	CMI (%)	Ol	Opx	Cpx	Sp	Phl
Z-5[a]	45.10	0.151	3.81	0.38	8.18	0.136	0.245	37.91	3.37	0.32	0.01	0.02	99.6	0.892	1.19	–0.6	54.6	26.8	16.2	2.4	
Z-6	46.18	0.184	4.59	0.43	7.73	0.13	0.241	36.60	3.54	0.34	0.03	0.01	99.9	0.894	1.04	1.0	46.0	34.0	17.1	2.9	
Z-7	45.27	0.157	3.82	0.39	7.96	0.13	0.254	37.91	3.33	0.33	0.03	0.01	99.5	0.894	1.18	–1.7	53.9	27.8	16.2	2.1	
Z-8	45.63	0.154	3.27	0.36	8.07	0.13	0.269	38.60	3.37	0.32	0.02	0.01	99.9	0.895	1.39	–1.2	55.9	26.6	16.0	1.5	
Z-9[a]	44.80	0.097	2.07	0.37	9.32	0.135	0.277	40.76	1.77	0.20	0.00	0.02	99.8	0.886	1.15	0.1	63.9	27.3	8.1	0.7	
Z-11	45.51	0.174	4.00	0.39	8.14	0.13	0.254	37.52	3.64	0.35	0.01	0.02	99.6	0.891	1.23	–0.1	52.9	27.5	17.3	2.3	
Z-12	45.34	0.123	3.26	0.42	7.86	0.13	0.275	39.74	2.75	0.26	0.01	0.01	99.9	0.900	1.14	–0.4	58.0	27.4	12.8	1.8	
Z-14	45.70	0.162	3.73	0.36	8.37	0.14	0.259	37.68	3.54	0.33	0.01	0.01	100.2	0.889	1.28	–0.4	52.9	28.4	16.8	1.9	
Z-15	45.94	0.181	4.29	0.43	7.86	0.13	0.244	37.16	3.55	0.31	0.01	0.01	99.8	0.894	1.12	–1.4	49.4	31.1	17.0	2.5	
Z-16	45.67	0.166	3.88	0.40	7.99	0.13	0.25	37.75	3.47	0.28	0.01	0.01	99.7	0.894	1.21	–0.3	51.9	29.3	16.5	2.3	
Z-17	45.25	0.140	3.62	0.36	8.05	0.13	0.264	38.70	3.05	0.26	0.01	0.01	99.4	0.895	1.14	–0.6	55.2	28.2	14.3	2.3	
Z-18	45.56	0.179	4.05	0.36	8.24	0.13	0.254	37.71	3.36	0.33	0.01	0.01	100.0	0.891	1.12	–0.3	52.5	28.8	16.4	2.3	
Z-65[a]	45.63	0.164	3.85	0.34	8.13	0.14	0.240	37.37	3.68	0.34	0.00	0.02	99.9	0.891	1.29	–0.3	52.0	28.5	17.4	2.1	
Z-71	45.02	0.149	3.65	0.37	8.25	0.13	0.266	39.01	3.26	0.29	0.01	0.01	100.1	0.894	1.20	0.4	57.4	24.7	15.7	2.2	
Z-72	44.87	0.154	3.53	0.35	8.20	0.13	0.257	38.60	3.14	0.29	0.03	0.01	99.5	0.893	1.20	0.4	57.3	25.4	15.1	2.2	
Hr-2	46.09	0.196	4.11	0.33	8.63	0.141	0.239	36.36	3.67	0.40	0.04	0.02	100.2	0.882	1.21	ND	48.5	31.8	17.6	2.2	
Hr-4	44.17	0.083	2.82	0.36	8.36	0.132	0.282	41.03	2.28	0.19	0.01	0.01	99.7	0.897	1.09	0.0	64.9	22.5	10.4	2.2	
Hr-6[a]	44.12	0.094	2.45	0.31	9.30	0.140	0.289	41.48	1.54	0.20	0.03	0.05	100.0	0.888	0.85	ND	67.2	24.6	6.6	1.7	
Hr-12	45.28	0.160	3.63	0.32	8.47	0.136	0.256	38.04	3.18	0.32	0.01	0.02	99.8	0.889	1.18	0.0	55.4	27.1	15.3	2.1	tr.
Hr-18	44.81	0.131	3.54	0.42	8.04	0.127	0.271	39.50	3.25	0.30	0.02	0.01	100.4	0.898	1.24	0.2	60.2	22.0	15.2	2.6	
Hr-20	45.20	0.167	3.90	0.36	8.27	0.134	0.258	38.10	3.21	0.34	0.03	0.03	100.0	0.891	1.11	–0.2	54.6	27.5	15.3	2.6	tr.
Hr-22	44.70	0.164	4.00	0.39	8.36	0.132	0.265	38.42	3.36	0.33	0.05	0.02	100.2	0.891	1.14	0.4	57.3	23.8	15.9	3.0	
Hr-25	44.08	0.167	3.62	0.35	13.06	0.183	0.241	35.35	2.98	0.43	0.08	0.02	100.2	0.828	1.11	–0.1	57.7	24.1	15.0	2.3	0.8
Hr-26	45.59	0.175	4.44	0.40	8.01	0.133	0.244	36.58	3.80	0.36	0.01	0.02	99.8	0.891	1.16	–0.1	49.4	29.5	18.3	2.8	
St-0	45.82	0.208	4.72	0.42	7.89	0.13	0.235	35.96	4.07	0.42	0.05	0.02	99.8	0.890	1.16	0.3	45.4	31.6	19.7	2.8	0.4
St-3	44.74	0.145	3.72	0.38	8.29	0.132	0.269	39.31	2.90	0.28	0.03	0.02	100.2	0.894	1.05	0.3	58.2	25.2	13.6	2.7	0.3
St-23	45.06	0.140	4.09	0.36	8.44	0.136	0.258	39.00	2.68	0.29	0.04	0.04	100.5	0.892	0.89	0.4	54.6	29.9	12.0	2.9	0.4
Ts-14	45.31	0.113	3.74	0.38	8.01	0.133	0.259	38.94	3.19	0.26	0.00	0.00	100.3	0.897	1.15	0.4	55.1	27.9	14.6	2.4	
Ts-21	44.94	0.152	3.91	0.36	8.34	0.134	0.256	38.16	3.12	0.30	0.01	0.01	99.7	0.891	1.08	0.3	55.2	27.4	14.7	2.7	tr.
Bosko	45.25	0.174	3.85	0.34	9.48	0.144	0.241	36.39	3.54	0.41	0.01	0.05	99.9	0.872	1.24	ND	51.0	30.2	17.2	1.5	
Aver. all	45.22	0.154	3.73	0.37	8.44	0.135	0.257	38.19	3.19	0.31	0.02	0.02	99.9	0.890	1.15		54.9	27.6	15.1	2.3	
Aver. 26	45.32	0.157	3.84	0.38	8.16	0.133	0.256	38.14	3.30	0.31	0.02	0.02	99.9	0.893	1.15		54.2	27.7	15.7	2.4	

Table 3 continued

	Whole-rock XRF analyses, wt.%:														Calculated mineral abundances, wt.%				
	SiO_2	TiO_2	Al_2O_3	Cr_2O_3	FeO	MnO	NiO	MgO	CaO	Na_2O	K_2O	P_2O_5	Total	Mg#	Ca/Al	CMI (%)	Ol	Opx	Cpx	Sp	Phl
Reference samples (harzburgite JP-1 and serpentinite UBN)																					
JP-1	44.26	0.01	0.71	0.44	7.77	0.124	0.322	46.86	0.55	0.00	0.00	0.00	101.0	0.915							
JP-1i	43.65	0.017	0.74	0.43	7.64	0.12	0.326	46.07	0.55	0.00	0.00	0.00	99.5	0.915		–2.4					
JP-1 RV	43.74	0	0.64	0.45	7.75	0.12	0.323	46.14	0.58	0.02	0.00	0.00	99.8	0.914							
UBN	45.57	0.11	3.36	0.39	8.46	0.143	0.295	40.43	1.36	0.21	0.03	0.02	100.4	0.895							
UBNi	45.33	0.12	3.33	0.39	8.45	0.14	0.294	40.24	1.37	0.13	0.02	0.006	99.8	0.895		–12					

Analyses of non-ignited reference samples were re-calculated to anhydrous compositions keeping the original totals. Averages are provided separately for all 30 samples and for 26 xenoliths, which have no strong Fe-enrichments

RV recommended values, *ND* not determined, *tr* trace amounts, *CMI* change of mass on ignition (positive values indicate weight gain in fresh samples due to oxidation of FeO to Fe_2O_3)

[a] Niigata analyses (eTable 2); all other data are from Mainz laboratory. JP-1i, UBNi, ignited reference samples

can be viewed as extensions of the latter towards the most pristine mantle compositions.

P-T estimates, mantle cross-section and a record of thermal history

Equilibration temperatures (*T*) were estimated from EPMA on cores and rims of pyroxene grains. The only garnet facies lherzolite in this study (Z-68) equilibrated at 1.96 GPa and 1,088°C from the Ca-opx thermometer of Brey and Köhler (1990) and the barometer of Nickel and Green (1985), i.e. the same techniques used earlier to establish *P-T* gradients for other central Asian xenolith suites: Vitim (Ionov et al. 2005a; Ionov et al. 1993) and Shavaryn–Tsaram (Ionov et al. 1998). Temperature estimates for spinel peridotites were obtained with the Ca-opx method and fixed pressure (*P*) of 1.5 GPa, the latter may cause uncertainties in *T* of up to 10° for *P* = 1.3–1.7 GPa.

The *T* estimates are given in Table 1 and plotted in Fig. 3 as histograms for each eruption centre. The xenoliths from Zala show the largest *T* range, 880–1,090°C, identical to that earlier obtained for spinel peridotites from Shavaryn–Tsaram. The single xenolith from Bosko equilibrated at 1,070°C. At three other sites, where no garnet-bearing xenoliths have been found, the *T* estimates do not exceed 1,005°C. Two-pyroxene thermometer of Wells (1977) yields *T* values close to those obtained by the Ca-opx(BK) method (within 20°C for 88% of the samples), like in many other well-documented spinel peridotite suites (Witt-Eickschen and O'Neill 2005), but the *T* differences are higher (20–40°C) for glass-bearing and strongly metasomatised rocks as well as samples with few (<8) opx core analyses (Table 1).

Assuming that temperature gradually increases with depth, one can infer relative positions of the xenoliths in the CLM cross-section. Moreover, equilibration pressures can be roughly estimated by projecting *T* estimates for each sample to the geotherm constructed previously using garnet-bearing xenoliths from Shavaryn–Tsaram (Ionov et al. 1998) and then to the *P* axis (Fig. 9a). The lowest *T* estimates in each of the five Tariat sites are very similar (~880°C; Fig. 3). The low-*T* peridotites are interpreted to represent the uppermost mantle; their cut-off *T* value corresponds to the temperature at the crust-mantle boundary (CMB) where peridotites replace granulites as the dominant rock type (Ionov et al. 1998; Stosch et al. 1995). Projection of the cut-off *T* value to the Tariat geotherm gives *P* ~ 1.3 GPa for the CMB. This corresponds to a depth of ~45 km assuming an average crustal density of ~2.8 g/cm^3 (Fig. 9a) in agreement with recent interpretations of regional geophysical data (Petit et al. 2002) but contrary to high crustal thicknesses (50–60 km) inferred

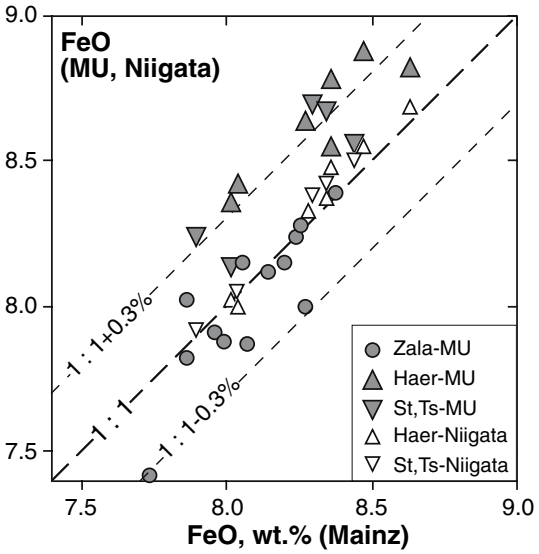

Fig. 5 FeO contents (wt. %) in whole-rock Tariat xenoliths obtained in Mainz plotted versus those from Niigata (*empty symbols*) and MU (*filled symbols*). The high-precision data from Niigata match those from Mainz very well (plotting close to the 1:1 reference line), but the conventional MU data show more scatter, with differences often exceeding 0.3% FeO

for Hangai by Zorin (1999). The similarity between the cut-off *T*-values for the five eruption sites (Fig. 3) indicates that the depth to the CMB is similar for all sampled localities in the area. The Zala xenoliths ($T \sim 880$–1,090°C) appear to provide continuous sampling of the spinel facies mantle from the CMB to the garnet lherzolite facies.

Temperature estimates obtained from pyroxene rims are higher than those obtained from core analyses for the majority of the xenoliths (Table 1) and appear to indicate heating in the mantle shortly (within thousands of years based on element diffusion rates, e.g. Werling and Altherr 1997) before the transport to the surface. The same heating event may have caused the formation of kelyphite after garnet in sample Z-68. By contrast, the lower contents of Al and Cr in the pyroxene rims relative to the cores are commonly attributed to cooling (Sachtleben and Seck 1981; Witt-Eickschen and Seck 1991) and thus seem to contradict the inference on heating based on the Ca contents. The two lines of evidence can be reconciled assuming that Ca diffuses much faster than Al and Cr in pyroxenes as inferred in some earlier xenolith and experimental studies (Klemme and O'Neill 2000; Werling and Altherr 1997; Witt-Eickschen and Seck 1991). In such a case, the mineralogical and EPMA data indicate that the Tariat CLM experienced slow, long-term cooling, possibly after a major crustal tectono-magmatic event in the late Paleozoic or the Mesozoic (Badarch et al. 2002; Jahn et al. 2004; Kovalenko et al. 2004) followed by rapid localised heating possibly related to the late Cenozoic volcanism.

Temperature and chemical effects on minor components in olivine

Temperature and pressure, in addition to bulk or mineral chemistry, are known to affect the distribution of some elements between olivine and pyroxenes or spinel (e.g. Hervig and Smith 1982; Köhler and Brey 1990; Stosch and Seck 1980) and hence their abundances in olivine. Indeed, the concentrations of Ca, Al and Cr in olivine from Tariat xenoliths are positively correlated with *T* estimates and are not related to Mg# (Fig. 10a, b). By contrast, those of Mn are negatively correlated with $Mg\#_{Ol}$ (Fig. 4d), but are not correlated with *T* values (not shown). Because the Tariat peridotites equilibrated in a broad *T* range (880–1,090°C) but show little chemical variation (generally low $Mg\#_{Ol}$ and $Cr\#_{Sp}$, high Al in cpx and bulk rocks), the data in this study (Table 2) can be used to constrain temperature effects on abundances of Ca, Al and Cr in olivine. Below, the Tariat data are considered together with high-precision EPMA obtained in the same laboratory on olivine from

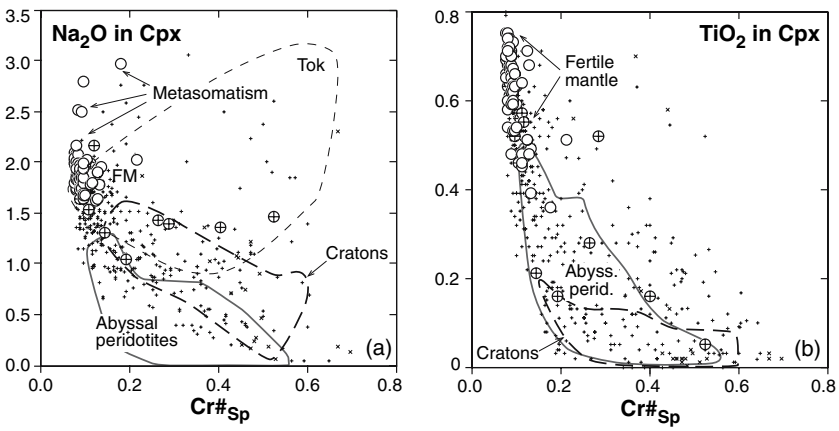

Fig. 6 Plots of $Cr\#_{Sp}$ versus Na_2O (**a**) and TiO_2 (**b**) in cpx (wt.%) in spinel peridotites from Tariat (conventional EPMA from eTable 1) and worldwide localities. *Symbols* and literature data sources are same as in Fig. 4. Tariat cpx usually have moderately high Na_2O and TiO_2 typical of fertile mantle (FM); rare $Na_2O \geq 2.2\%$ are due to metasomatic enrichments, enrichments in TiO_2 are not common

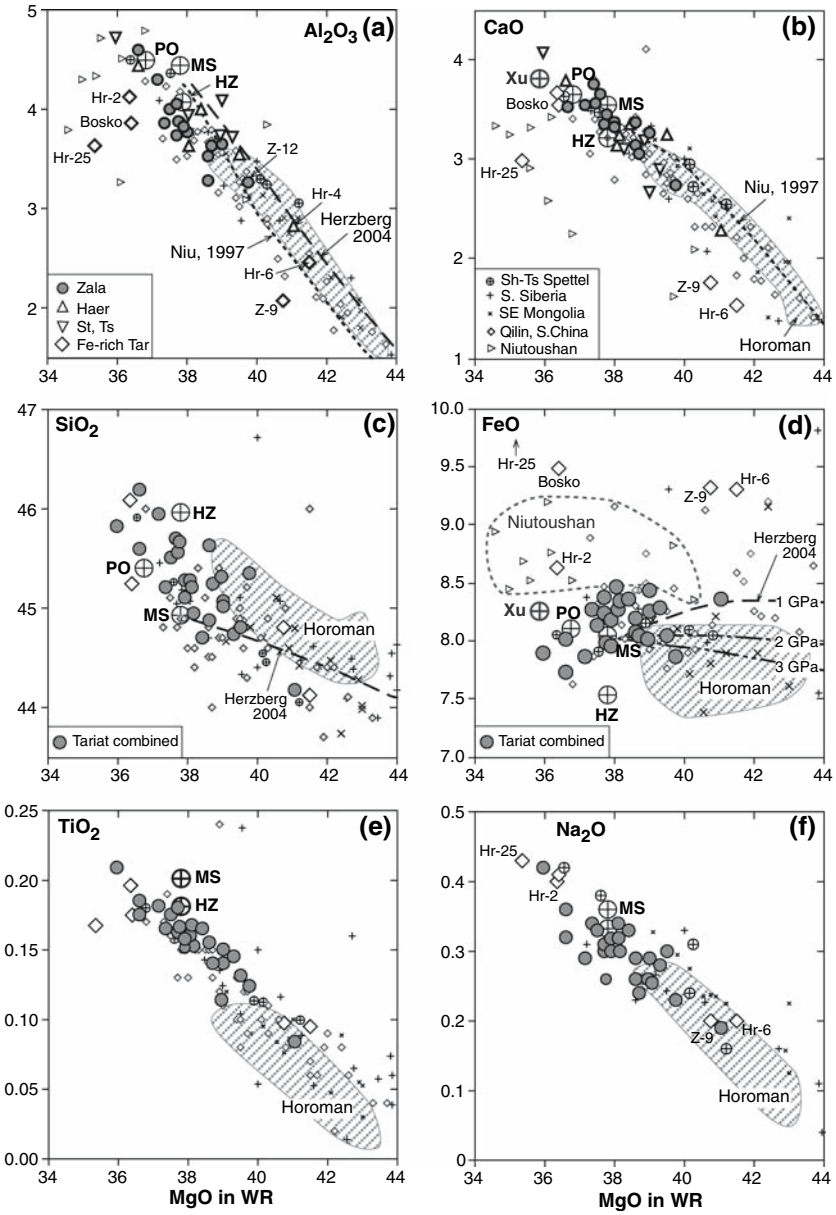

Fig. 7 Plots of MgO versus major and minor oxides (wt. %) in whole-rock Tariat xenoliths (high-precision data, Table 3); Fe-enriched Tariat xenoliths are labelled. Note that xenoliths from Zala (*small filled circles*), Haer (*triangles*) and Shute and Tsagan (*upside-down triangles*) are shown separately in **a** and **b**, but together in **c**–**f** (as *large filled circles*). Also shown are peridotite xenoliths from Shavaryn–Tsaram (Spettel et al. 1991), southern Siberia (Ionov et al. 2005a; Ionov et al. 2005c), south-eastern Mongolia (Wiechert et al. 1997) and SE China (Qi et al. 1995; Xu et al. 2000) as well as Horoman massif peridotites (*hatched field*, Takazawa et al. 2000). Large crossed circles are primitive mantle estimates after Hart and Zindler (1986) (HZ), McDonough and Sun (1995) (MS), Palme and O'Neill (2003) (PO) and Xu et al. (2000). *Dashed black lines* show residues from fractional melting of fertile spinel lherzolite at 1–3 GPa (Herzberg 2004; Niu 1997). Note high FeO reported for some xenoliths from SE China (Niutoushan and Mingxi based on defocused EPMA of fused rock powders)

lherzolite-harzburgite (LH) series xenoliths from Tok in SE Siberian craton (Ionov et al. 2005c), which equilibrated in a more narrow *T* interval but cover a broader range of major element compositions.

Because the *T* values (Table 1) are estimated from Ca in pyroxenes, the excellent CaO_{ol}-*T* correlation for the Tariat olivines ($r^2 = 0.97$; Fig. 10b) indicates that olivine and pyroxene cores are well equilibrated regardless of minor Ca zoning in pyroxene rims (eTable 1). On the basis of experimental data, Köhler and Brey (1990) argued that partitioning of Ca between olivine and cpx is controlled both by *T* and *P* and proposed a Ca-in-ol barometer for *P* = 1–6 GPa. Yet, its application to spinel peridotites commonly yields erratic *P* estimates (e.g. Witt-Eickschen and O'Neill 2005). Our data do not enable direct assessment of the role of pressure in the ol-cpx Ca exchange, but the robust linear CaO_{ol}-*T* trend obtained for the Tariat xenoliths (Fig. 10b) further indicates that temperature, rather than pressure, is the dominant parameter controlling CaO_{ol} in spinel lherzolites (at *P* ~ 1.3–1.8 GPa, Fig. 9).

Many Tok xenoliths match the Tariat CaO_{ol}-*T* trend but olivine in some Tok harzburgites has lower Ca at given *T* (Fig. 10d), possibly due to incomplete equilibration with cpx or Ca-phosphates (Ionov et al. 2006) of late-stage metasomatic origin. CaO contents in olivine from Eifel xenoliths (Witt-Eickschen and O'Neill 2005) fall in the field of the Tariat and Tok olivine at moderate *T* values but show a broad range (0.04–0.06%) at <900°C (Fig. 10d).

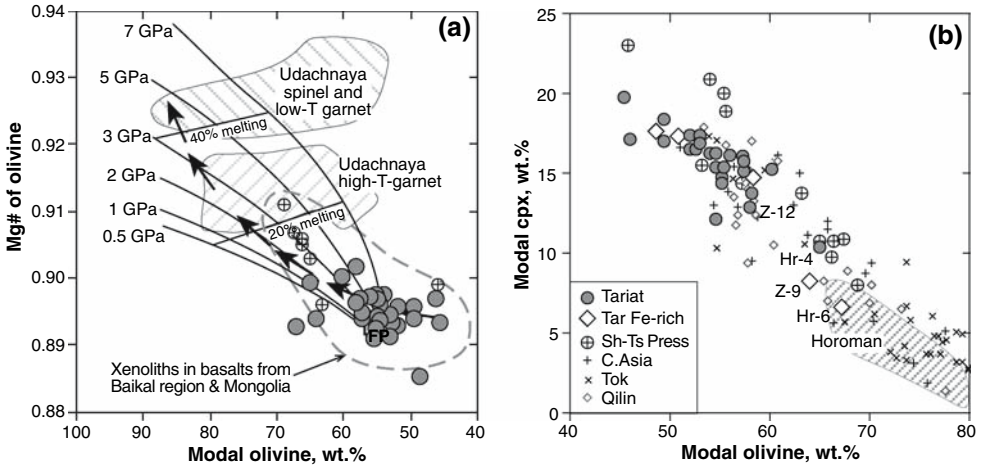

Fig. 8 Plots of modal olivine versus $Mg\#_{Ol}$ (**a**) and modal cpx (**b**). Also shown in a are fields for peridotite xenoliths from the Udachnaya kimberlite on the Siberian craton (Boyd et al. 1997) and from alkali basalts in central Asia (Ionov et al. 2005c), the ''oceanic trend'' (*arrows*) after Boyd (1989) and batch partial melt extraction residues (*solid black lines*) from fertile peridotite at 0.5–7 GPa (Walter 1999; 2003). Data for Shavaryn–Tsaram are from Press et al. (1986); sources and *symbols* for other data are same as in Fig. 7

The most likely reason for the latter is insufficient precision of the EPMA data for the Eifel olivine at low Ca, which is commonly the case in routine EPMA.

The good linear correlations between T values and Al_2O_3 ($r^2 = 0.92$) and Cr_2O_3 ($r^2 = 0.75$) in Tariat olivines (Fig. 10b) indicate that the abundances of Al and Cr in mantle olivine, similar to Ca, are affected by temperature. Unlike for Ca, however, the abundances of Al and Cr are ultimately controlled by ol-spl exchange and must also depend on Cr/(Cr + Al) in coexisting spinel, i.e. the most (Al,Cr)-rich phase. $Cr\#_{Sp}$ is linked to melt extraction degrees during the formation of residual peridotites from pristine mantle and shows a broad variation range in CLM (0.07–0.7, Figs. 4a, 6). This contrasts with the narrow variation range for CaO in cpx (usually 17–22%), which does not depend on melting degrees and is mainly controlled by temperature. Thus, major element composition of peridotites is likely to affect the abundances of Cr and Al in olivine much more than those of Ca. Indeed, olivine Z-9 from the only Tariat xenolith with relatively Cr-rich spinel ($Cr\#_{Sp}$ 0.21 vs. 0.07–0.12 in all other samples; Table 1 and Fig. 4a) has much more Cr_2O_3 (0.029%) than any other Tariat olivine (≤ 0.018%) and plots above the T-Cr_{ol} trend (but on the T-Ca_{ol} trend) in Fig. 10b and d. Furthermore, olivines from refractory, Cr-rich Tok peridotites contain much more Cr than the Tariat olivines at similar T (Fig. 10d) but usually have lower Al. Tariat olivine Hr-25 (with very low Mg#) has an anomalously high Al content (Fig. 10b). A Cr-Al plot (Fig. 10c) clearly distinguishes olivines from fertile peridotites, which define a T-controlled positive correlation ($r^2 = 0.81$ for the Tariat xenoliths), and olivines from refractory peridotites characterized by a broad range of Cr at low Al.

Overall, the combined Tariat-Tok dataset demonstrates that the abundances of Cr and Al in mantle olivine are sensitive both to temperature and mineral or whole-rock chemistry. Witt-Eickschen and O'Neill (2005) reported a positive Cr_{Ol}-T correlation for 16 spinel peridotites (mainly from Eifel) but failed to establish a link between Cr_{Ol} and $Cr\#_{Sp}$. I note that none of the peridotites in their study are fertile and nearly all (14 out of 16) have Cr-rich spinel ($Cr\#_{Sp}$ ≥0.2) and $Mg\#_{Ol}$ ≥0.913. The Cr abundances reported for those Eifel olivines are higher than in the Tariat olivines at similar T (870°C < T <1,100°C) but close to those from Tok (Fig. 10d), i.e. consistent with equilibration with Cr-rich spinel. Thus, the refractory peridotite suite in the study of Witt-Eickschen and O'Neill (2005) does not appear to be appropriate to explore the effects of $Cr\#_{Sp}$ on Cr_{Ol} because of a narrow compositional range in combination with a very broad T range (870–1,220°C) and hence prevailing temperature effects.

The role of partial melting in the origin of CLM beneath Tariat

In spite of their mainly fertile character and narrow compositional range, the Tariat peridotites define conspicuous trends on modal (Fig. 8) and major element plots (Figs. 4, 6, 7). Such trends can result from several processes: (1) variable degrees of melt extraction from pristine mantle; (2) metamorphic differentiation or ''modal banding'' (Palme and O'Neill 2003); (3) tectonic mingling with pyroxenites (Bodinier 1988; Kaeser et al. 2006); (4) variable degrees of ''re-fertilization'' in the CLM (Bodinier and Godard 2003; Simon et al. 2003).

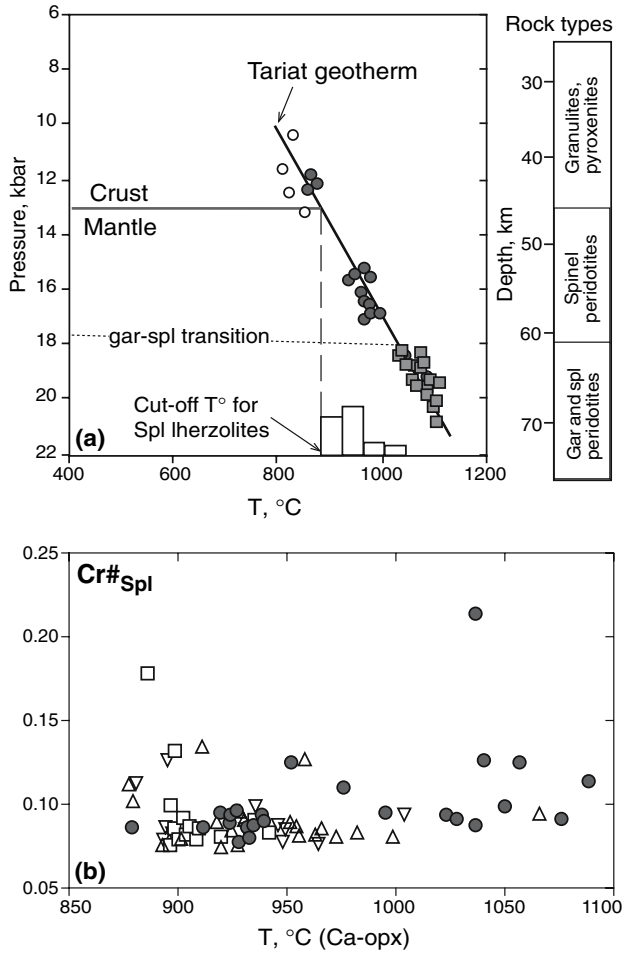

Fig. 9 **a** A geotherm and lithospheric cross-section for the Tariat region constructed from *P-T* data on garnet-bearing xenoliths from Shavaryn–Tsaram (modified after Ionov et al. 1998): *empty circles*, garnet granulites; *filled circles*, garnet pyroxenites; *filled squares*, garnet-bearing peridotites. The depth of origin for individual Tariat xenoliths can be obtained by projecting their *T* estimates (see a simplified histogram, like those in Fig. 3, superposed on the horizontal axis) onto the geotherm and then to the pressure-depth axis. **b** A plot of $Cr\#_{Sp}$ versus equilibration *T*-values (Ca-opx, Brey and Köhler 1990) as a proxy for the depth of origin (data from Table 1): Zala, *filled circles*; Haer, *triangles*; Shute, *upside down triangles*; Tsagan, *squares*. Note that the $Cr\#_{Sp}$ (hence melt extraction degrees) are not related to depth either for individual eruption centres or the whole Tariat series

The partial melting concept is most commonly invoked to explain modal and chemical variations in peridotite suites (Frey and Prinz 1978; McDonough and Sun 1995; Nickel and Green 1984; Pearson et al. 2003), and it agrees well with modal and chemical data on the Tariat xenoliths. Co-variations of MgO versus Al_2O_3 and CaO as well as co-variations of modal olivine versus modal cpx generally match experimental melting trends (Herzberg 2004; Niu 1997; Walter 2003) and plot at extensions of modal and chemical co-variation trends for other peridotite series, which represent well-documented residues of moderate to high degrees of partial melting from primitive mantle sources (Figs. 7, 8).

Crucial evidence in favour of a partial melting origin for the Tariat peridotites comes from the fact that the contents and ratios of elements sensitive to melt extraction define clear and coherent trends (except for Fe-enriched samples) both for whole-rock and mineral data. In particular, $Mg\#_{Ol}$ is positively correlated with $Cr\#_{Sp}$ and negatively correlated with Al_2O_3 in cpx and MnO in olivine (Fig. 4). Samples with either most refractory or most fertile whole-rock compositions also define depleted or fertile end-members on mineral trends, e.g. Z-12 and Hr-4 with highest whole-rock MgO and lowest Al_2O_3 (Figs. 7a, 11) also have highest $Mg\#_{Ol}$ and $Cr\#_{Sp}$ (Fig. 4b), lowest modal cpx (Fig. 8b) and MnO in olivine (Fig. 4d), and some of the lowest Al_2O_3 and TiO_2 in cpx (Figs. 4c, 6b). This rules out an origin for the whole-rock variations by segregation of minerals because the mineral and whole-rock trends are not likely to be consistent in the modal banding or mingling models as discussed below.

Modal heterogeneity on centimetre scale, e.g. diffuse bands enriched in cpx or olivine, is common in peridotite massifs, like Lherz or Horoman (Bodinier and Godard 2003). While similar bands or patches were also reported in mantle xenoliths worldwide (e.g. Boyd and Mertzman 1987; Ionov 2004; Irving 1980; Kaeser et al. 2006), they are difficult to identify in cm-size, coarse-grained peridotite nodules. Such ''hidden'' modal variations, in particular cpx enrichments post-dating partial melting and unrelated to extent of melt extraction are often invoked as a major factor in modal and major element variations in fertile mantle peridotites because they may produce linear trends on bulk rock co-variation diagrams similar to those caused by melt extraction (Palme and Nickel 1985). Metamorphic differentiation may be the only mechanism, except for metasomatism, that is capable of producing mantle peridotites with higher contents of Ca and Al than in primitive mantle models (Hart and Zindler 1986; Jagoutz et al. 1979; Palme and O'Neill 2003).

Press et al. (1986) found that some Shavaryn–Tsaram peridotites deviate from trends defined by the remainder of their samples on chemical and modal co-variation diagrams versus $Mg\#_{Ol}$ or whole-rock MgO and attributed such features to ''mechanical mixing'' unrelated to mineral-liquid equilibria, i.e. addition of 2–6% cpx to melting residues. As noted above, this is not the case with the Tariat xenoliths in this study, which define a common modal olivine-cpx trend with the majority of other xenoliths from central and east Asia (Fig. 8b).

Extent of melt extraction and melting conditions for the Tariat peridotites however can hardly be defined in detail because of insufficient experimental data on low-degree

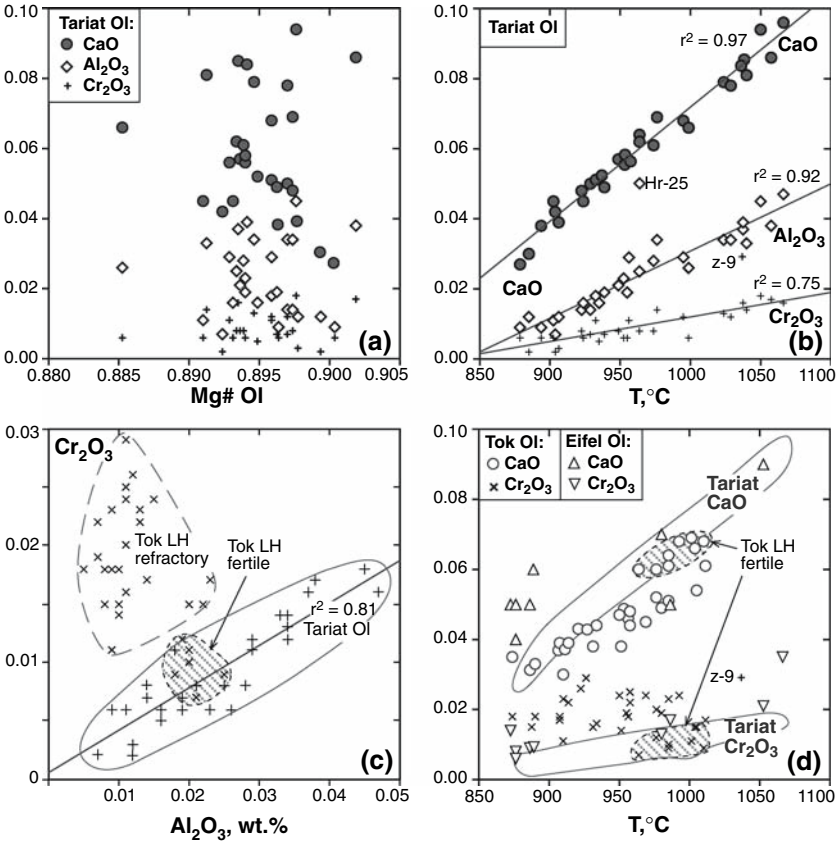

Fig. 10 The contents of CaO, Al_2O_3 and Cr_2O_3 in olivine (wt. %, EPMA from Table 2) plotted versus $Mg\#_{Ol}$ (**a**), equilibration temperature (Ca-opx, Brey and Köhler 1990) (**b**, **d**), and Cr_2O_3 plotted versus Al_2O_3 (**c**). Linear regression lines and correlation coefficients for Tariat olivines are given in **b** and **c** (samples Hr-25 and Z-9 were omitted in regressions for Al and Cr, respectively, see text). Also shown are data for olivine from LH series xenoliths from Tok, SE Siberia (Ionov et al. 2005c) and Eifel, Germany (Witt-Eickschen and O'Neill 2005). The contents of Ca, Al and Cr in fertile Tok xenoliths (*hatched fields*) fall within the trends for the Tariat olivines. By contrast, olivines in Tariat sample Z-9 and refractory peridotites from Tok and Eifel contain much more Cr indicating that its abundances in mantle olivines are controlled both by *T* and Cr/(Cr + Al) values in coexisting spinel and bulk rocks

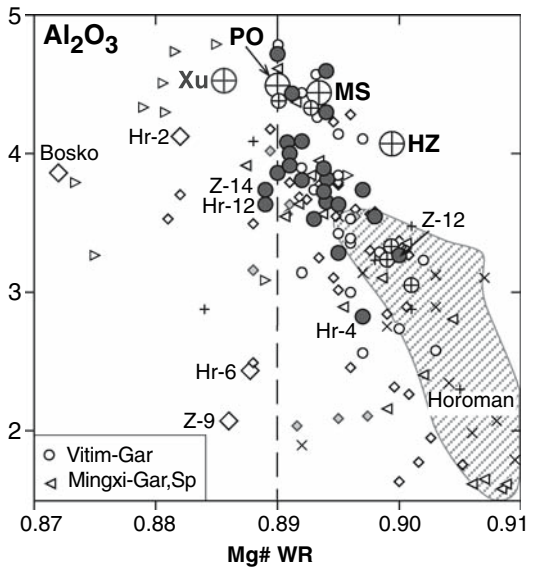

Fig. 11 Plot of Al_2O_3 (wt. %) versus Mg# in whole-rock (WR) Tariat xenoliths (high-precision data from Table 3); Tariat xenoliths likely to be enriched in Fe are labelled. Shown for comparison are spinel and garnet lherzolite xenoliths from central and east Asia (Ionov et al. 2005a; Xu et al. 2000), other data and symbols are same as in Fig. 7. Note a broad Al_2O_3 range for fertile ($Mg\#_{WR}$ 0.890–0.895) Tariat xenoliths and a broad scatter of $Mg\#_{WR}$ in the literature data on Chinese xenoliths

melting of very fertile mantle. Some Tariat lherzolites plot off experimental melt extraction trends (Fig. 7a–d), possibly due to the generally lower MgO abundances, combined with either higher or lower Al_2O_3, SiO_2, FeO contents than in experimental starting compositions (Herzberg 2004; Niu 1997; Walter 2003).

Another issue is the range of FeO in the Tariat xenoliths. Excluding five Fe-enriched samples labelled in Fig. 7d, the xenoliths range from 7.73 to 8.47 wt.% FeO, with an average of 8.14 ± 0.20% (1 σ). Although the latter value is within the error of the worldwide average for mantle peridotites (8.1 ± 0.05%) compiled by O'Neill and Palme (1998), the reasons for broad variations in FeO (hence Mg#) at given MgO (e.g. 7.86–8.47% FeO at MgO ~38%, Fig. 7d) are not clear. Likewise, the contents of Al_2O_3 in fertile Tariat xenoliths range from 3.63 to 4.72% at $Mg\#_{WR}$ 0.890 ± 0.001 (Fig. 11) whereas both parameters are considered robust melt extraction indices and are expected to be negatively correlated. Because iron contents in melting residues increase as melting proceeds at <2 GPa and decrease at higher pressures, the FeO scatter in the Tariat suite can be reconciled with experimental data assuming that melting took place at a range of pressures (1–3 GPa; Fig. 7d) and that primitive mantle contains 1–2% less MgO than the starting compositions of Herzberg (2004). Minor

additions of iron by metasomatism may also contribute to the FeO variations as discussed in the next section.

The contents of Ni in whole-rock Tariat peridotites (Ni_{WR}) are positively correlated with MgO (eFig. 2a), which is commonly seen in peridotite suites the world over and linked to Ni compatibility in olivine-rich residues during melt extraction (McDonough and Sun 1995; Nickel and Green 1984; Palme and O'Neill 2003). By contrast, Ni in olivine (Ni_{Ol}) shows no clear correlation with Ni_{WR} or $Mg\#_{Ol}$ (eFig. 2b, c), which may be taken as indicating that higher Ni in Mg-rich peridotites is due to higher modal olivine alone and imply no Ni-enrichments in residual olivine during partial melting. The latter contradicts experimental and natural data (Sobolev et al. 2005 and refs. therein). Fertile Tok xenoliths ($Mg\#_{Ol}$ 0.890–0.905), like the Tariat samples, show no Ni_{Ol}-$Mg\#_{Ol}$ trend (eFig. 2c) in spite of the NiO_{Ol} variation range well beyond the precision of individual EPMA (±0.003–0.007% NiO). The complete Tok suite however shows a significant increase in NiO_{Ol} from ~0.36 to ~0.39% as $Mg\#_{Ol}$ increases from 0.89 to 0.92 (eFig. 2c). We attribute the NiO_{Ol} variations in the Tariat and other fertile peridotites to variable contents of accessory Fe-Ni sulfides and hence variable degrees of Ni partitioning from olivine to those sulfides (Fleet and Stone 1990; Li et al. 2003); in more refractory rocks, primary sulfides are rare because sulfur is exhausted during melt extraction.

Metasomatism and major element compositions in the Tariat mantle

Several lines of evidence indicate that some Tariat xenoliths were strongly enriched in iron after the melting event, which formed their protoliths. Four samples have whole-rock FeO ≥ 9.3%, i.e. ≥1% above any estimates for primitive mantle (Palme and O'Neill 2003) or experimental residues of melt extraction from fertile peridotites at any pressure (Herzberg 2004; Walter 2003). Some of these and other Tariat xenoliths have heterogeneous Fe distribution (Table 2) in olivine cores and/or Fe-zoning in mineral rims (eTable 1). Importantly, the Fe-enriched samples have lower $Mg\#_{Ol}$ relative to the melting-related $Mg\#_{Ol}$ versus $Cr\#_{Sp}$ trend (Fig. 4b) defined by the remainder of the xenoliths. These features were likely caused by interaction of residual peridotites with evolved, low-Mg# mafic silicate melts (Bodinier and Godard 2003; Lee and Rudnick 1999). Such melts may contain as much FeO as the peridotites but have low Cr solubilities (Liu and O'Neill 2004), hence they can enrich the host peridotites in iron but cannot significantly affect their Cr/Al at low to moderate melt/rock ratios. The strong Fe-enrichments are found both in olivine-rich and fertile Tariat xenoliths (Figs. 7, 8b) whereas refractory peridotites are believed to be more permeable for melt percolation and prone to metasomatism (e.g. Bodinier et al. 1988; Ionov et al. 2005b; McDonough and Frey 1989).

While strong enrichments in iron are evident for several Tariat xenoliths discussed above, it is much less clear if the same process also affected other Tariat peridotites on a smaller scale. Some of the FeO variation outlined in the previous section might have been caused by minor additions of iron by metasomatism, which are too small to be identified with certainty using petrologic criteria. Such minor Fe-enrichments could be invoked for two peridotites with lowest $Mg\#_{WR}$ (0.889) among fertile Tariat xenoliths in Fig. 11 (Z-14 and Hr-12). These two samples have fairly low Al_2O_3 (3.6–3.7%) indicating higher partial melting degrees than for other fertile Tariat xenoliths; yet, they deviate slightly towards lower Mg# both from the whole-rock Mg#-Al_2O_3 trend (Fig. 11) and from the $Mg\#_{Ol}$ vs. $Cr\#_{Sp}$ trend (Fig. 4b) attributed to melt extraction.

None of the Fe-enriched Tariat peridotites have unusually high contents of Ca, Na or Ti (Fig. 7) and many (Z-9, Bosko, Hr-6) contain no accessory amph, phl or silicate glass. Thus, the Fe-enrichments in the Tariat suite were not accompanied by precipitation of cpx or the ''hydrous'' phases (modal metasomatism). In this regard, it is distinct from peridotite suites, in which Fe-enrichments accompanied transformation of lherzolites and harzburgites into wehrlites (Ionov et al. 2005b; Lee and Rudnick 1999). Similarly, the Fe-enrichments do not appear to have been accompanied by a decrease in Ni abundances, e.g. Fe-enriched xenoliths Hr-6 and Z-9 are among three Tariat samples with highest whole-rock NiO (eFig. 2a).

Tariat CLM: homogeneous or heterogeneous?

The data on over 70 xenoliths from four Tariat eruption centres in this study, together with published results on xenoliths from Shavaryn–Tsaram, outline CLM compositions in a domain, which extends ~20 km from north to south and ~10 km east–west (Fig. 1b) in the depth range ~45 to ≥60 km (Fig. 9), i.e. between 15 and 20 km below the crust-mantle boundary. These data enable to (1) reliably characterize the CLM domain beneath the Tariat volcanic field and (2) explore heterogeneities within this domain in 3D space.

This study shows that the CLM 'sampled' by peridotite xenoliths in the Tariat area has a limited range of modal and chemical variation dominated by fertile compositions. In a more general sense, it indicates that individual off-craton CLM domains may have narrow variation ranges on a scale of ≥10–20 km. The generally fertile CLM compositions obtained here for Tariat broadly match those

observed in xenoliths hosted by alkali basalts south and east of Lake Baikal (Ionov 2002; Ionov et al. 2005a) thus indicating that the CLM in a broad area between central Mongolia and the southern rim of the Siberian craton (Fig. 1a) may be generally fertile.

Another important issue is whether the limited compositional variations in the Tariat CLM are randomly distributed in 3D space or, alternatively, define lateral or vertical trends or heterogeneities. The ranges and averages of modal and major oxide abundances are similar for all five main Tariat xenolith sites (Table 1; Fig. 7a, b). Furthermore, several chemical parameters (e.g. $Cr\#_{Sp}$, Fig. 9b) show no correlation with equilibration temperatures (i.e. the depth of origin, Fig. 9a). Thus, the Tariat CLM appears to be homogeneous, both laterally and vertically, on km-scale in terms of modal and major element compositions; grain size and microstructures in the majority of the xenoliths are not very different either (Fig. 2).

The distribution of accessory amph and phl and spongy cpx however shows lateral km-scale heterogeneities, i.e. the volatile-bearing minerals are either absent (Zala) or occur in different combinations in xenoliths from different eruption centres (only phl in Shute, rare phl in Haer and Shavaryn–Tsaram, mainly amph in Tsagan). These features probably reflect minor metasomatic events induced by upward migration of small amounts of fluids with different abundances of water, CO_2, alkalies; fluid compositions may have also evolved during percolation through the mantle (e.g. Barry et al. 2003; Ionov et al. 2002).

Because Tariat is situated close to the centre of Asia and has not been affected by events operating at plate boundaries since mid-Phanerozoic and probably earlier (Badarch et al. 2002; Zorin 1999), amph and phl in the Tariat CLM likely formed by intra-plate processes (Barry et al. 2003). Furthermore, the uneven lateral distribution of the volatile-bearing phases in the Tariat mantle indicates that their formation and assemblages may be related to local, small-scale events and sources rather than regional tectonic settings. The example of the Tariat xenoliths further demonstrates that it may be erroneous to consider the very presence of amph and phl in mantle rocks as indicators of subduction-related metasomatism (e.g. Szabo et al. 2004) even though amph and phl are believed to be common in the mantle wedge above subducting slabs (e.g. Ionov and Hofmann 1995; McInnes et al. 2001).

Veins and patches of silicate glass found in some Tariat xenoliths appear to reflect local melting related to heterogeneously distributed fluid and heat sources (e.g. magma conduits) in the CLM shortly before the eruption that brought the xenoliths to the surface (Ionov et al. 1994). Alternatively, such features have been attributed to transport-related ''decompression melting'' of metasomatic phases (e.g. Yaxley and Kamenetsky 1999) but the latter hypothesis disregards the fact that all mantle xenoliths experience decompression during the transport but only few show in-situ melting. The presence and proportions of glass in the Tariat xenoliths are not related to their equilibration temperatures and therefore depth of origin and decompression rates. For example, several Tariat xenoliths with abundant (>10%) melt pockets come from the uppermost and coldest CLM ($T \leq 900$°C, based on cores of opx) whereas some xenoliths with higher equilibration temperatures (St-12, $T = 1004$°C), hence deeper origin and higher decompression rates, contain unmelted phl.

Analytical uncertainties and assessment of CLM heterogeneities

This section seeks to evaluate the impact of analytical uncertainties on inferences concerning the origin and chemical variations of the CLM. As shown above, conventional XRF analyses of the Tariat peridotites may differ significantly from the high-precision data on the same samples. Regarding published data on xenoliths from Shavaryn–Tsaram, XRF analyses of five lherzolites reported by Spettel et al. (1991) fall in the FeO range and the Mg-Al field (eFig. 1) defined by the Tariat data from Mainz. By contrast, analyses of Shavaryn–Tsaram lherzolites reported by Press et al. (1986) tend to have higher Al_2O_3 and/or MgO than those from Spettel et al. (1991) and Tariat data in this work (eFig. 1a), as well as generally lower FeO (average FeO = 7.74% vs. 8.16% for Tariat samples without strong Fe-enrichments in this work). Overall, the XRF data for Tariat xenoliths from Mainz and Niigata match each other well whereas those from MU, as well as published data on Shavaryn–Tsaram xenoliths, display broad ranges of Al and Fe at given Mg indicating significant inter-laboratory bias for those elements (also for Si, Cr, Na; eTable 3).

Based on the MU Tariat data and those from Press et al. (1986) for Shavaryn–Tsaram, one might infer that the two peridotite suites define distinct Mg-Al trends (eFig. 1a) and thus have different sources and/or melting histories. Such differences, however, are not seen when comparing the Tariat data from Mainz with those for Shavaryn–Tsaram after Spettel et al. (1991). Likewise, Press et al. (1986) noted that FeO in their Shavaryn–Tsaram dataset are consistently lower than for San Carlos xenoliths, SW USA (Frey and Prinz 1978) and interpreted them as reflecting ''bulk chemical differences in primitive mantle the suites were derived from''. By contrast, Palme and O'Neill (2003) found only minor differences in average FeO contents in many CLM peridotite suites worldwide. New high-precision analyses of Shavaryn–Tsaram peridotites are required to resolve the controversy. Yet, the data in this study

strongly indicate that analytical bias may have contributed to the range of FeO and Mg# reported for mantle peridotites worldwide. On the other hand, Fe-enrichments similar to those documented in the Tariat suite are real and may be common in some CLM domains, e.g. SE Siberian craton or some localities in SW USA (Ionov et al. 2005c; Smith 2000).

Uncertainties of determining Mg# in olivine and pyroxenes by conventional EPMA may be significant compared to the narrow Mg# range (0.89–0.92) estimated for residual off-craton peridotites (e.g. Bodinier and Godard 2003; Pearson et al. 2003; Walter 2003). The EPMA data on the Tariat xenoliths (Fig. 4a, b) indicate that $Mg\#_{Ol}$ variations of ~0.005 due to analytical uncertainties may be common in conventional EPMA datasets on mantle rocks; such uncertainties may be an important but poorly defined factor in the variations of $Mg\#_{Ol}$ reported for fertile spinel lherzolites the world over (Fig. 4a).

The quality of analytical data for Fe and Mg can be assessed by plotting whole-rock Mg# versus $Mg\#_{Ol}$. Because olivine is a major host of Mg and Fe in spinel peridotites, $Mg\#_{Ol}$ is often assumed to be identical to $Mg\#_{WR}$ (e.g. Palme and O'Neill 2003). Ionov et al. (2005c) recently reported a tight ($r^2 = 0.995$) linear $Mg\#_{Ol}$–$Mg\#_{WR}$ correlation for xenoliths from Tok (except Fe-enriched samples), with $Mg\#_{WR}$ slightly lower than $Mg\#_{Ol}$ (up to 0.005 in most fertile rocks). The Tariat data from Mainz (obtained with the same methods as the Tok dataset) show $Mg\#_{WR} < Mg\#_{Ol}$ as well and plot along the low-Mg# part of the Tok trend (Fig. 12a). I concur with the inference of the earlier work (Ionov et al. 2005c) that $Mg\#_{WR} < Mg\#_{Ol}$ is likely due to the presence of spinel (2–3% in fertile lherzolites), whose Mg# is much lower than in coexisting olivine (0.78 vs. 0.89 in fertile Tariat xenoliths) at similar FeO contents (~10%).

By contrast to the Mainz dataset, a $Mg\#_{Ol}$–$Mg\#_{WR}$ plot for the xenoliths in this study based on EPMA and XRF from MU defines only a vague trend, with data points on both sides of 1:1 reference line (Fig. 12b). Data on Shavaryn–Tsaram peridotites published two decades ago (Ionov 1986; Press et al. 1986) are similarly dispersed on the same diagram, as is common in literature data on mantle rocks obtained by routine techniques. The mismatch between $Mg\#_{Ol}$ and $Mg\#_{WR}$ reported in the literature can be spectacular, e.g. for peridotite xenoliths from Huinan (Xu et al. 2003) (Fig. 12c). This is often the case for whole-rock data obtained by wet chemistry or EPMA of fused powders (Qi et al. 1995), not to mention cases when Fe_2O_3 values are mistakenly reported as FeO (F.-Y. Wu, personal communication 2006).

I conclude that while high-precision XRF and EPMA data are crucial to establish the origin of mantle peridotites, some published data are not of adequate quality. Inferences on regional and world-wide chemical variation in the CLM, in particular Mg#, may be influenced by analytical uncertainties. Establishing systematic linear correlations between $Mg\#_{Ol}$ and $Mg\#_{WR}$ in residual peridotites provides a good means of demonstrating the quality of the data.

Major element composition of primitive mantle

The composition of the earth's primitive mantle was initially estimated using more or less arbitrarily selected cpx-rich peridotite xenoliths from different localities (Jagoutz et al. 1979). A problem with this procedure is that high

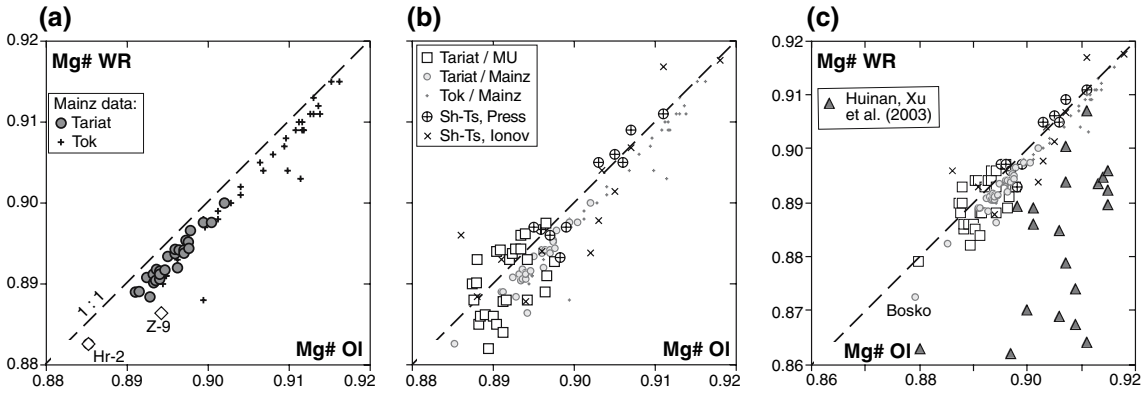

Fig. 12 $Mg\#_{Ol}$ versus whole-rock Mg# ($Mg\#_{WR}$) for Tariat peridotite xenoliths based on data from Mainz (**a**) and MU as well as literature data for Shavaryn–Tsaram peridotites (Ionov 1986; Press et al. 1986) (**b**); data from b are compared in **c** with those reported for peridotites from Huinan (Xu et al. 2003). The high-precision data from Mainz define a tight linear correlation in **a**, with $Mg\#_{Ol} < Mg\#_{WR}$ (*dashed line* shows equal $Mg\#_{Ol}$ and $Mg\#_{WR}$); the correlation matches the trend earlier reported for xenoliths from Tok (Ionov et al. 2005c). Rare Fe-enriched peridotites (labelled) plot off the trend due to heterogeneous Fe distribution in olivine. Mg# from conventional analytical methods (**b**) show broad scatter (both below and above the 1:1 line) and may have errors ≥0.005. Low quality of some literature Mg# data for mantle peridotites and their olivine is particularly evident in **c**

modal cpx may be due to enrichments rather than very low melt extraction degrees (Hart and Zindler 1986; McDonough and Sun 1995; Palme and Nickel 1985) as likely is the case with some cpx-rich Shavaryn–Tsaram xenoliths (Press et al. 1986). A better approach may be to select least depleted and least metasomatised rocks from well-studied fertile peridotite suites after identifying and deleting anomalous samples enriched by late-stage processes because such samples are likely to plot off melt extraction trends for those suites (Figs. 4, 8b).

The Tariat suite is one of the most appropriate fertile peridotite series for that purpose. The contents of Al, Ca, Si, Ti, Na in many xenoliths in this study (Fig. 7) are much alike or higher than estimates for primitive mantle (PM) (Palme and O'Neill 2003 and references therein). Furthermore, the Tariat xenoliths have some of the lowest $Cr\#_{Sp}$ and $Mg\#_{Ol}$, highest Al_2O_3 and TiO_2 in cpx (Figs. 4, 6) as well as highest modal cpx and lowest modal olivine among residual mantle peridotites worldwide, e.g. they overlap the fertile end of the ''oceanic trend'' (Boyd 1989) (Fig. 8). Samples with Fe-enrichments are identified here from combined whole-rock and EPMA data; other major oxides show little, if any, metasomatic effects.

Four PM estimates are shown together with Tariat xenoliths in Figs. 7, 11 and eFig. 2a. The estimate of Hart and Zindler (1986) has significant discrepancies with the Tariat chemical co-variation trends, in particular the content of FeO is lower than in any Tariat xenolith (Fig. 7d), the Mg# and NiO are too high (Fig. 11, eFig. 2a) while CaO and Al_2O_3 are low (Fig. 7a, b) in comparison with most fertile Tariat rocks. The PM composition of McDonough and Sun (1995) fits the Tariat suite quite well except for somewhat high MgO, Mg# (Fig. 11) and NiO (eFig. 2) and low SiO_2 (Fig. 7). The recent PM estimate by Palme and O'Neill (2003) matches best both the Tariat co-variation trends and the compositions of the most fertile Tariat lherzolites. In particular, the $Mg\#_{WR} = 0.890$ in that model is identical to the lowest $Mg\#_{WR}$ among the fertile Tariat xenoliths (except Fe-enriched) and is close (±0.003) to $Mg\#_{WR}$ reported for most fertile xenoliths from Vitim (Fig. 11). Thus the Tariat data support the $Mg\#_{WR}$ value of 0.890 for PM and indicate that mantle peridotites with $Mg\#_{WR} < 0.890$ (assuming good analytical quality) likely experienced post-melting Fe-enrichments.

Xu et al. (2000) suggested a primitive mantle composition based on the mean of ten ''most fertile, fresh, large xenoliths'' from SE China, excluding lherzolites containing metasomatic minerals; all of them have $Mg\#_{WR} < 0.890$. Compared to three other PM estimates shown in Figs. 7 and 11, the values for MgO (35.87%) and Mg_{WR} (0.8856) proposed by Xu et al. (2000) are much lower while those for FeO (8.26%) and CaO (3.8%) are higher. The MgO of 35.87% is lower than in any xenolith in this study except the strongly Fe-enriched Hr-25. Some samples from Xu et al. (2000) have anomalous compositions, e.g. consistently high FeO and low CaO and Mg# in the Niutoushan and some Mingxi xenoliths (Figs. 7a–d, 11). I note that Xu et al. (2000) did not demonstrate the quality of their analytical data and do not appear to have screened their sample selection (not indicated in their paper) for enrichments in Fe and Ca (cpx). The latter may have much stronger chemical impact than small amounts of accessory amph or phl as shown here and in other peridotite studies (Bodinier and Godard 2003; Ionov et al. 2005b; Lee and Rudnick 1999). Overall, xenolith-based PM estimates, like that of Xu et al. (2000), can be misleading if they disregard the importance of data quality and proper screening for metasomatic contributions.

Several studies found a tendency to high Ca/Al in fertile mantle peridotites compared to the chondritic value of ~1.1 (Hart and Zindler 1986; McDonough and Sun 1995; O'Neill and Palme 1998); Palme and Nickel (1985) obtained a mean Ca/Al of 1.25, i.e. ~15% higher than the chondrite average. Ca/Al in the Tariat suite ranges from 0.85 to 1.39, with an average of 1.15 ± 0.10 (1 σ); >2/3 of the samples fall within 10% of the chondritic Ca/Al (Table 3). While the Tariat average is slightly super-chondritic, the difference is negligible compared to uncertainties of both estimates. McDonough and Sun (1995) argued that low melt extraction degrees may cause small increases in Ca/Al in the residues. Thus, the data in this study do not support the notion that Ca/Al in pristine mantle is significantly above the chondritic value. Rather, metasomatism and late-stage alteration may be responsible for high Ca/Al reported for some CLM peridotites. For example, 0.5 wt.% of secondary calcite in a lherzolite with 3 wt.% CaO increases its Ca/Al by 0.09; precipitation of cpx with high Ca/Al is a common feature of mantle metasomatism (e.g. Ionov et al. 2005b; Pearson et al. 2003; Yaxley et al. 1991).

The reasons for the unusually fertile character of the Tariat CLM are hard to constrain based on results of this study alone. The most likely option is low degrees of melt extraction in an intra-plate setting but it remains to be explained why the partial melting degrees were so low. Accretion of convecting asthenosphere to the bottom of early lithosphere due to conductive cooling (without partial melting) seems to be possible as well but the range of major element compositions in the asthenospheric mantle is poorly constrained, and small-degree melting in very fertile upwelling material during the accretion may be a better alternative. Barry et al. (2003) suggested that parental magmas of Tariat volcanic rocks could be produced by extraction of low-degree melts from a near-primitive, amphibole-bearing source. Such an origin for the Tariat CLM appears to be consistent with results of this study. The oldest crustal rocks exposed in central Mongolia

south and north of Hangai have Proterozoic to Archean ages (Badarch et al. 2002; Cunningham 2001; Kovalenko et al. 2004) indicating that the Tariat CLM may have formed in the Precambrian.

Conclusions

1. Spinel peridotite xenoliths in alkali basaltic rocks from Tariat in central Mongolia are dominated by fertile lherzolites and constitute one of the least refractory CLM suites the world over. Chemical compositions of the most fertile Tariat lherzolites are close to the primitive mantle estimate of Palme and O'Neill (2003) and indicate an $Mg\#_{WR} = 0.890$ for the PM.
2. Modal and major element variations in the Tariat suite indicate an origin by low degrees of melt extraction from the PM, probably at 1–3 GPa, and are not consistent with alternative mechanisms, like metamorphic segregation or tectonic mingling.
3. Some Tariat peridotites were enriched in iron by percolation of evolved silicate melts, with no or little metasomatic effects on other major and minor oxides or modal compositions.
4. The Tariat CLM is homogeneous both laterally (within 10–20 km) and vertically (depth range ~45 to ≥60 km) in terms of modal and major element compositions. The distribution of accessory (<1%) amph and phl however shows km-scale lateral heterogeneities.
5. High-precision EPMA show that the contents of Ca in olivine are mainly controlled by temperature (at $P = 1.3–1.8$ GPa) whereas the contents of Al and Cr depend both on T values and Cr/Al in bulk peridotites and/or coexisting spinel.
6. Comparisons of conventional and high-precision XRF and EPMA on the Tariat xenoliths together with literature examples emphasize the need for high-quality major element data on mantle peridotites, in particular Mg#, to constrain their origin. Analytical uncertainties in published work contribute substantially to chemical heterogeneities inferred for the CLM.

Acknowledgments I am grateful to A. Hofmann, E. Takazawa and J.-L. Bodinier for support in Mainz, Niigata and Montpellier and thank *T.* Bradley, A. Friedrichsen, K. Furuta, N. Groschopf, A. Gurenko, D. Kuzmin, C. Lawson, C. Merlet, N. Pearson, A. Sobolev for analytical and technical assistance and advice. Altantsetseg, Boyar, Chimid, A. Goreglyad, W. Griffin, V. Kovalenko, S. O'Reilly participated in field work. The research was supported by funding from the Soviet-Mongolian Geologic Expedition (defunct), Australian Research Council (including Australian Research Fellowship and Grants to DAI), Australian Academy of Sciences, Japan Society for the Promotion of Science, Max-Planck-Society (Germany) and French CNRS (UMR 5568 and 6524). I thank two anonymous reviewers and the editor for helpful comments.

References

Badarch G, Cunningham WD, Windley BF (2002) A new terrane subdivision for Mongolia: implications for the Phanerozoic crustal growth of Central Asia. J Asian Earth Sci 21:87–110

Barry TL, Kent RW (1998) Cenozoic magmatism in Mongolia and the origin of central and east Asian basalts. In: Flower MJF, Chung S-L, Lo C-H, Lee TY (eds) Mantle dynamics and plate interactions in East Asia. Amer Geophys Union Geodynamics Series 27, Washington, pp 347–366

Barry TL, Saunders AD, Kempton PD, Windley BF, Pringle MS, Dorjnamjaa D, Saandar S (2003) Petrogenesis of Cenozoic basalts from Mongolia: evidence for the role of asthenospheric versus metasomatized lithospheric mantle sources. J Petrol 44:55–91

Bodinier JL (1988) Geochemistry and petrogenesis of the Lanzo peridotite body, western Alps. Tectonophysics 149:67–88

Bodinier J-L, Godard M (2003) Orogenic, ophiolitic and abyssal peridotites. In: Carlson RW (ed) Treatise on Geochemistry. The mantle and core, vol 2. Elsevier, Amsterdam, pp 103–170

Bodinier JL, Dupuy C, Dostal J (1988) Geochemistry and petrogenesis of Eastern Pyrenean peridotites. Geochim Cosmochim Acta 52:2893–2907

Boyd FR (1989) Compositional distinction between oceanic and cratonic lithosphere. Earth Planet Sci Lett 96:15–26

Boyd FR, Mertzman SA (1987) Composition and structure of the Kaapvaal lithosphere, Southern Africa. In: Mysen BO (ed) Magmatic processes: physicochemical principles. Geochem Soc Spec Publ, vol 1, pp 3–12

Boyd FR, Pokhilenko NP, Pearson DG, Mertzman SA, Sobolev NV, Finger LW (1997) Composition of the Siberian cratonic mantle: evidence from Udachnaya peridotite xenoliths. Contrib Mineral Petrol 128:228–246

Brey GP, Köhler T (1990) Geothermobarometry in four-phase lherzolites II. New thermobarometers, and practical assessment of existing thermobarometers J Petrol 31:1353–1378

Cunningham WD (2001) Cenozoic normal faulting and regional doming in the southern Hangay region, Central Mongolia: implications for the origin of the Baikal rift province. Tectonophysics 331:389–411

Delvaux D, Moeys R, Stapel G, Melnikov A, Ermikov V (1995) Paleostress reconstructions and geodynamics of the Baikal region, Central Asia, Part I. Palaeozoic and Mesozoic pre-rift evolution. Tectonophysics 252:61–101

Fleet ME, Stone WE (1990) Nickeliferous sulfides in xenoliths, olivine megacrysts and basaltic glass. Mineral Petrol 105:629–636

Frey FA, Prinz M (1978) Ultramafic inclusions from San Carlos, Arizona: petrologic and geochemical data bearing on their petrogenesis. Earth Planet Sci Lett 38:129–176

Genshaft YS, Klimenko GV, Saltykovsky AY, Ageeva LI (1990) New data on the composition and age of Cenozoic volcanics in Mongolia (in Russian). Trans (Doklady) USSR Acad Sci Earth Sci Sect 311:420–424

Hart SR, Zindler A (1986) In search of a bulk-Earth composition. Chem Geol 57:247–267

Hervig RL, Smith JV (1982) Temperature-dependent distribution of Cr betwen olivine and pyroxenes in lherzolite xenoliths. Contrib Mineral Petrol 81:184–189

Herzberg C (2004) Geodynamic information in peridotite petrology. J Petrol 45:2507–2530

Ionov DA (1986) Spinel peridotite xenoliths from the Shavaryn–Tsaram volcano, northern Mongolia: petrography, major element chemistry and mineralogy. Geol Carpath 37:681–692

Ionov D (2002) Mantle structure and rifting processes in the Baikal-Mongolia region: geophysical data and evidence from xenoliths in volcanic rocks. Tectonophysics 351:41–60

Ionov DA (2004) Chemical variations in peridotite xenoliths from Vitim, Siberia: inferences for REE and Hf behaviour in the garnet facies upper mantle. J Petrol 45:343–367

Ionov DA, Hofmann AW (1995) Nb-Ta-rich mantle amphiboles and micas: implications for subduction-related metasomatic trace element fractionations. Earth Planet Sci Lett 131:341–356

Ionov DA, Borisovsky SE, Kovalenko VI, Ryabchikov ID (1983) Micas from mantle nodules in alkali basalts from Mongolia. Trans (Doklady) USSR Acad Sci Earth Sci Sect 269:1189–1192

Ionov DA, Borisovsky SE, Kovalenko VI, Ryabchikov ID (1984) First find of amphibole in mantle xenoliths in alkali basalts from Mongolia (in Russian). Trans (Doklady) USSR Acad Sci 276:238–242

Ionov DA, Ashchepkov IV, Stosch H-G, Witt-Eickschen G, Seck HA (1993) Garnet peridotite xenoliths from the Vitim volcanic field, Baikal region: the nature of the garnet-spinel peridotite transition zone in the continental mantle. J Petrol 34:1141–1175

Ionov DA, Hofmann AW, Shimizu N (1994) Metasomatism-induced melting in mantle xenoliths from Mongolia. J Petrol 35:753–785

Ionov DA, O'Reilly SY, Griffin WL (1997) Volatile-bearing minerals and lithophile trace elements in the upper mantle. Chem Geol 141:153–184

Ionov DA, O'Reilly SY, Griffin WL (1998) A geotherm and lithospheric cross-section for central Mongolia. In: Flower MJF, Chung S-L, Lo C-H, Lee TY (eds) Mantle dynamics and plate interactions in East Asia. Amer Geophys Union Geodynamics Ser 27, Washington, DC, pp 127–153

Ionov DA, Bodinier J-L, Mukasa SB, Zanetti A (2002) Mechanisms and sources of mantle metasomatism: major and trace element compositions of peridotite xenoliths from Spitsbergen in the context of numerical modeling. J Petrol 43:2219–2259

Ionov DA, Ashchepkov I, Jagoutz E (2005a) The provenance of fertile off-craton lithospheric mantle: Sr-Nd isotope and chemical composition of garnet and spinel peridotite xenoliths from Vitim, Siberia. Chem Geol 217:41–75

Ionov DA, Chanefo I, Bodinier J-L (2005b) Origin of Fe-rich lherzolites and wehrlites from Tok, SE Siberia by reactive melt percolation in refractory mantle peridotites. Contrib Mineral Petrol 150:335–353

Ionov DA, Prikhodko VS, Bodinier J-L, Sobolev AV, Weis D (2005c) Lithospheric mantle beneath the south-eastern Siberian craton: petrology of peridotite xenoliths in basalts from the Tokinsky Stanovik. Contrib Mineral Petrol 149:647–665

Ionov DA, Hofmann AW, Merlet C, Gurenko AA, Hellebrand E, Montagnac G, Gillet P, Prikhodko VS (2006) Discovery of whitlockite in mantle xenoliths: inferences for water- and halogen-poor fluids and trace element residence in the terrestrial upper mantle. Earth Planet Sci Lett 244:201–217

Irving AJ (1980) Petrology and geochemistry of composite ultramafic xenoliths in alkalic basalts and implications for magmatic processes within the mantle. Am J Sci 280-A:389–426

Jagoutz E, Palme H, Baddenhausen H, Blum K, Cendales M, Dreibus G, Spettel B, Lorenz V, Wänke H (1979) The abundances of major, minor and trace elements in the Earth's mantle as derived from primitive ultramafic nodules. Geochim Cosmochim Acta suppl 11, 2 (Proc Lunar Planet Sci Conf 10th), pp 2031–2050

Jahn B-m, Windley B, Natal'in B, Dobretsov N (2004) Phanerozoic continental growth in Central Asia. J Asian Earth Sci 23:599–603

Jarosewich E, Nelen JA, Norberg J (1980) Reference samples for electron microprobe analysis. Geostand Newsl 4:43–47

Kaeser B, Kalt A, Pettke T (2006) Evolution of the lithospheric mantle beneath the Marsabit volcanic field (northern Kenya): constraints from textural, P-T and geochemical studies on xenoliths. J Petrol 47:2149–2184

Kepezhinskas VV (1979) Cenozoic alkaline basaltoids of Mongolia and their deep-seated inclusions (in Russian). Nauka, Moscow, pp 312

Klemme S, O'Neill HSC (2000) The effect of Cr on the solubility of Al in orthopyroxene: experiments and thermodynamic modelling. Contrib Mineral Petrol 140:84–98

Köhler TP, Brey GP (1990) Calcium exchange between olivine and clinopyroxene calibrated as a geothermobarometer for natural peridotites from 2 to 60 kb with applications. Geochim Cosmochim Acta 54:2375–2388

Kovalenko VI, Yarmolyuk VV, Kovach VP, Kotov AB, Kozakov IK, Salnikova EB, Larin AM (2004) Isotope provinces, mechanisms of generation and sources of the continental crust in the Central Asian mobile belt: geological and isotopic evidence. J Asian Earth Sci 23:605–627

Lee C-T, Rudnick RL (1999) Compositionally stratified cratonic lithosphere: petrology and geochemistry of peridotite xenoliths the Labait volcano, Tanzania. In: Gurney JJ, Gurney JL, Pascoe MD, Richardson SH (eds) Proceedings of the 7th international Kimberlite conference, vol 1. RedRoof design, Cape Town, pp 503–521

Li C, Ripley EM, Mathez EA (2003) The effect of S on the partitioning of Ni between olivine and silicate melt in MORB. Chem Geol 201:295

Liu X, O'Neill HSC (2004) The effect of Cr_2O_3 on the partial melting of spinel lherzolite in the system CaO-MgO-Al_2O_3-SiO_2-Cr_2O_3 at 1.1 GPa. J Petrol 45:2261–2286

McDonough WF (1990) Constraints on the composition of the continental lithospheric mantle. Earth Planet Sci Lett 101:1–18

McDonough WF, Frey FA (1989) Rare earth elements in upper mantle rocks. In: Lipin BR, McKay GA (eds) Geochemistry and mineralogy of rare earth elements. Mineral Soc Amer, Washington, pp 99–145

McDonough WF, Sun S-s (1995) The composition of the Earth. Chem Geol 120:223–253

McInnes BIA, Gregoire M, Binns RA, Herzig PM, Hannington MD (2001) Hydrous metasomatism of oceanic sub-arc mantle, Lihir, Papua New Guinea: petrology and geochemistry of fluid-metasomatised mantle wedge xenoliths. Earth Planet Sci Lett 188:169–183

Nickel KG, Green DH (1984) The nature of the upper-most mantle beneath Victoria, Australia as deduced from ultramafic xenoliths. In: Kornprobst J (ed) Kimberlites II. The Mantle and Crust-Mantle relationships. Elsevier, Amsterdam, pp 161–178

Nickel KG, Green DH (1985) Empirical geothermobarometry for garnet peridotites and implications for the nature of the lithosphere, kimberlites and diamonds. Earth Planet Sci Lett 73:158–170

Niu Y (1997) Mantle melting and melt extraction processes beneath ocean ridges: Evidence from abyssal peridotites. J Petrol 38:1047–1074

Niu Y, Langmuir CH, Kinzler RJ (1997) The origin of abyssal peridotites: a new perspective. Earth Planet Sci Lett 152:251–265

O'Neill HSC, Palme H (1998) Composition of the silicate Earth: implications for accretion and core formation. In: Jackson I (ed) The Earth's Mantle: structure, composition and evolution—the Ringwood volume. Cambridge University Press, Cambridge, pp 3–126

O'Reilly SY, Griffin WL (1988) Mantle metasomatism beneath Victoria, Australia: I. Metasomatic processes in Cr-diopside lherzolites. Geochim Cosmochim Acta 52:433–447

Palme H, Nickel KG (1985) Ca/Al ratio and composition of the Earth's mantle. Geochim Cosmochim Acta 49:2123–2132

Palme H, O'Neill HSC (2003) Cosmochemical estimates of mantle composition. In: Carlson RW (ed) Treatise on Geochemistry. The mantle and core, vol 2. Elsevier, Amsterdam, pp 1–38

Pearson DG, Canil D, Shirey SB (2003) Mantle samples included in volcanic rocks: xenoliths and diamonds. In: Carlson RW (ed) Treatise on Geochemistry. The mantle and core, vol 2. Elsevier, Amsterdam, pp 171–276

Petit C, Déverchère J, Calais E, San'kov V, Fairhead D (2002) Deep structure and mechanical behavior of the lithosphere in the Hangai-Hövsgöl region, Mongolia: new costraints from gravity modeling. Earth Planet Sci Lett 197:133–149

Press S, Witt G, Seck HA, Eonov DA, Kovalenko VI (1986) Spinel peridotite xenoliths from the Tariat Depression, Mongolia. I Major element chemistry and mineralogy of a primitive mantle xenolith suite. Geochim Cosmochim Acta 50:2587–2599

Priestley K, Debayle E, McKenzie D, Pilidou S (2006) Upper mantle structure of eastern Asia from multimode surface waveform tomography. J Geophys Res 111. doi:10.1029/2005JB004082

Qi Q, Taylor LA, Zhou X (1995) Petrology and geochemistry of mantle peridotite xenoliths from SE China. J Petrol 36:55–79

Sachtleben T, Seck HA (1981) Chemical control of Al-solubility in orthopyroxene and its implications on pyroxene geothermometry. Contrib Mineral Petrol 78:157–165

Simon NSC, Irvine GJ, Davies GR, Pearson DG, Carlson RW (2003) The origin of garnet and clinopyroxene in ''depleted'' Kaapvaal peridotites. Lithos 71:289–322

Smith D (2000) Insights into the evolution of the uppermost continental mantle from xenolith localities on and near the Colorado Plateau and regional comparisons. J Geophys Res 105:16769–16781

Sobolev AV, Hofmann AW, Sobolev SV, Nikogosian IK (2005) An olivine-free mantle source of Hawaiian shield basalts. Nature 434:590–597

Spettel B, Palme H, Ionov DA, Kogarko LN (1991) Variations in the iridium content of the upper mantle of the Earth. Lunar Planet Sci Conf XXII:1301–1302

Stosch H-G, Seck HA (1980) Geochemistry and mineralogy of two spinel peridotite suites from Dreiser Weiher, West Germany. Geochim Cosmochim Acta 44:457–470

Stosch H-G, Lugmair GW, Kovalenko VI (1986) Spinel peridotite xenoliths from the Tariat Depression, Mongolia. II: geochemistry and Nd and Sr isotopic composition and their implications for the evolution of the subcontinental lithosphere. Geochim Cosmochim Acta 50:2601–2614

Stosch H-G, Ionov DA, Puchtel IS, Galer SJG, Sharpouri A (1995) Lower crustal xenoliths from Mongolia and their bearing on the nature of the deep crust beneath central Asia. Lithos 36:227–242

Szabo C, Falus G, Zajacz Z, Kovacs I, Bali E (2004) Composition and evolution of lithosphere beneath the Carpathian-Pannonian Region: a review. Tectonophysics 393:119–137

Takazawa E, Frey FA, Shimizu N, Obata M (2000) Whole rock compositional variations in an upper mantle peridotite (Horoman, Hokkaido, Japan): are they consistent with a partial melting process. Geochim Cosmochim Acta 64:695–716

Takazawa E, Okayasu T, Satoh K (2003) Geochemistry and origin of the basal lherzolites from the northern Oman ophiolite (northern Fizh block). Geochem Geophys Geosyst 4. doi:10.1029/2001GC000232

Tapponier P, Molnar P (1979) Active faulting and Cenozoic tectonics of the Tien Shan, Mongolia, and Baikal regions. J Geophys Res 84:3425–3459

Walter MJ (1999) Melting residues of fertile peridotite and the origin of cratonic lithosphere. In: Fei Y, Bertka CM, Mysen BO (eds) Mantle petrology: field observations and high-pressure experimentation. Spec Publ Geochem Soc 6, Houston, pp 225–239

Walter MJ (2003) Melt extraction and compositional variability in mantle lithosphere. In: Carlson RW (ed) Treatise on Geochemistry. The mantle and core, vol 2. Elsevier, Amsterdam, pp 363–394

Wells PRA (1977) Pyroxene thermometry in simple and complex systems. Contrib Mineral Petrol 62:129–139

Werling F, Altherr R (1997) Thermal evolution of the lithosphere beneath the French Massif Central as deduced from geothermobarometry on mantle xenoliths. Tectonophysics 275:119–141

Wiechert U, Ionov DA, Wedepohl KH (1997) Spinel peridotite xenoliths from the Atsagin-Dush volcano, Dariganga lava plateau, Mongolia: a record of partial melting and cryptic metasomatism in the upper mantle. Contrib Mineral Petrol 126:345–364

Windley BF, Allen MB (1993) Mongolian Plateau: evidence for a late Cenozoic mantle plume under central Asia. Geology 21:295–298

Witt-Eickschen G, O'Neill HSC (2005) The effect of temperature on the equilibrium distribution of trace elements between clinopyroxene, orthopyroxene, olivine and spinel in upper mantle peridotite. Chem Geol 221:65–101

Witt-Eickschen G, Seck HA (1991) Solubility of Ca and Al in orthopyroxene from spinel peridotite: an improved version of an empirical geothermometer. Contrib Mineral Petrol 106:431–439

Xu X, O'Reilly SY, Griffin WL, Zhou X (2000) Genesis of young lithospheric mantle in southeastern China: an LAM-ICPMS trace element study. J Petrol 41:111–148

Xu Y-G, Menzies MA, Thirlwall MF, Huang X-L, Liu Y, Chen X-M (2003) ''Reactive'' harzburgites from Huinan, NE China: products of the lithosphere-asthenosphere interaction during lithospheric thinning? Geochim Cosmochim Acta 67:487–505

Yarmolyuk VV, Kovalenko VI, Ivanov VG, Samoylov VS (1995) Dynamics and magmatism of late Mesozoic-Cenozoic mantle hot spot, southern Khangai (Mongolia). Geotectonics 28:391–407

Yaxley GM, Kamenetsky V (1999) In situ origin for glass in mantle xenoliths from southeastern Australia: insights from trace element compositions of glasses and metasomatic phases. Earth Planet Sci Lett 172:97–109

Yaxley GM, Crawford AJ, Green DH (1991) Evidence for carbonatite metasomatism in spinel peridotite xenoliths from western Victoria, Australia. Earth Planet Sci Lett 107:305–317

Zorin YA (1999) Geodynamics of the western part of the Mongolia-Okhotsk collisional belt, Trans-Baikal region (Russia) and Mongolia. Tectonophysics 306:33–56